Regional Air Quality Modeling System (RAQMS) predictions of the tropospheric ozone budget over East Asia

Pierce, R. B.[1], J. A. Al-Saadi[1], T. Schaack[2], A. Lenzen[2], T. Zapotocny[2], D. Johnson[2], C. Kittaka[2], M. Buker[2], M. H. Hitchman[2], G. Tripoli[2], T. D. Fairlie[1], J. R. Olson[1], M. Natarajan[1], J. Crawford[1], J. Fishman[1], M. Avery[1], E. V. Browell[1], J. Creilson[3],Y. Kondo[4], S.T. Sandholm[5]

[1] NASA Langley Research Center, Hampton, Va

[2] University of Wisconsin, Madison, Wi

[3] SAIC, Hampton, Va

[4] University of Tokyo, Tokyo Japan

[5] Georgia Institute of Technology, Atlanta, Ga

Submitted to the TRACE-P Special Issue, JGR, November 15, 2002

Abstract: The National Aeronautics and Space Administration (NASA) Langley Research Center (LaRC) and University of Wisconsin (UW) Regional Air Quality Modeling System (RAQMS) is used to estimate the tropospheric ozone budget over East Asia during the NASA Global Tropospheric Experiment (GTE) TRAnsport and Chemical Evolution over the Pacific (TRACE-P) mission. The computed ozone budget explicitly accounts for stratosphere/troposphere exchange (STE) and in-situ ozone production using online chemical calculations. The East Asian O_3 budget is computed during the period from March 07th to April 12th, 2001. Gross formation dominates STE by a ratio of 7 to 1 in East Asia during TRACE-P. However, this ratio is strongly influenced by altitude of the tropopause. Approximately 30% of the ozone that is advected across the tropopause over East Asia is subsequently advected out over the Western Pacific within the upper 4km of the troposphere by the Japan jet. The average net photochemical production (gross formation – gross destruction) within the regional domain is 0.37 Tg/day, or 7% of the average flux at the eastern boundary of the domain during the TRACE-P time period. The budget analysis shows a very close balance between sources and sinks within the RAQMS regional domain during the TRACE-P time period. This balance results in very small average accumulation (~1 Tg) of O_3 in the East Asian region and very little net export averaged over the period (0.03 Tg/day). The low ozone export from East Asia predicted by RAQMS during TRACE-P is a consequence of relatively high dry deposition rates, which are 37% of the gross ozone formation (1.469 Tg/day) within the TRACE-P regional domain.

1. Introduction

The global tropospheric ozone budget is composed of two primary sources: input from the stratosphere and in situ photochemical generation. The relative importance of these two sources has been the focus of numerous studies throughout the past three decades [e.g., Fishman and Crutzen, 1978; Fishman, 1985; Wang et al., 1998]. It is clear that there are specific times of the year and regions around the planet where one source term is dominant. For example, high levels of ozone in the upper free troposphere downwind from a region of cyclogenesis and tropopause folding are likely the result of stratosphere-troposphere exchange [e.g. Danielsen et al., 1987]. Conversely, high concentrations in the planetary boundary layer where a large high pressure system has dominated the weather pattern for several days are likely the result of efficient photochemical generation of ozone from pollution. The relative importance of these sources during spring in East Asia is less clear. Quantifying the East Asian tropospheric ozone budget during the spring 2001 TRAnsport and Chemical Evolution over the Pacific (TRACE-P) mission is the focus of this study.

The TRACE-P mission was conducted by the Global Tropospheric Experiment (GTE) of the National Aeronautics and Space Administration (NASA) during February through April 2001. The goals of TRACE-P included determining the chemical composition of Asian outflow, quantifying the export of chemically and radiatively important gases, determining the chemical evolution of the outflow, and understanding the processes which control its evolution [Jacob et al., this issue]. TRACE-P observational goals were accomplished through an intensive measurement campaign conducted with the NASA DC8 and P3B aircraft and ground based instrumentation.

Figure 1 shows the climatological (1979-2000) February-April tropospheric ozone residual (TOR; http://asd-www.larc.nasa.gov/TOR/data.html) derived from the difference between Total Ozone Mapping Spectrometer (TOMS) total column ozone measurements (http://toms.gsfc.naa.gov/ozone/ozone.html) and Solar Backscatter UltraViolet (SBUV) stratospheric column measurements [Fishman and Balok, 1999]. The East Asian TOR shows high tropospheric column ozone (>40 DU) over the Ganges River valley and Central China. This high ozone appears to be advected over the western

Pacific Ocean between 35^{o} and 40^{o}N. The East Asian components of the DC8 and P3B flights during TRACE-P are indicated by bold lines in Figure 1. The flights were primarily within the East China Sea, Sea of Japan and Western Pacific. The prevailing off-shore flow during this time period [Fuelberg, this issue] indicates that the TRACE-P flights were down-wind of regions with large industrial emissions, such as Shanghai, Beijing, and Seoul, and to the north of climatological biomass burning regions in Thailand, Cambodia, and Vietnam [Duncan et al, 2002]. However, large quantities of ozone are also brought down from the stratosphere in this region during the spring [Carmichael et al., 1998].

Carmichael et al. [1998] used the Sulfur Transport Eulerian Model (STEM-II) regional-scale transport/chemistry model to assess the relative importance of downward transport from the upper troposphere and in-situ production in determining the ozone distribution in East Asia during May 1-15, 1987. They found that high ozone levels near 1-2 km above the surface, observed in association with frontal passages, were largely determined by downward fluxes from the upper troposphere, particularly north of 30°N. In-situ chemical production generally dominated below 1km, with more than 50% of the ozone produced by anthropogenic emissions of precursors, primarily NO_x, over S. E. China, Taiwan, Korea, the Japan Sea, and central Japan.

Liu et al. [2002] used the Goddard Earth Observing System CHEMical transport model (GEOS-CHEM) [Bey et al., 2001a] to quantify anthropogenic and natural influences on East Asian ozone. High ozone mixing ratios observed by ozoneondes during March in the lower troposphere over Hong Kong were shown to be strongly influenced by East Asian biomass burning events. Stratospheric influences were most pronounced in the upper troposphere over Hong Kong during January through April. Liu et al. [2002] estimate that anthropogenic (biomass+fossil fuel) emissions from East Asia result in eastward ozone fluxes at 150^{o}E which peak at ~0.575 Tg/day when integrated from 10^{o}N to 60^{o}N during March. Bey et al. [2001b] used GEOS-CHEM to interpret measurements taken during the February-March 1994 GTE Pacific Exploratory Mission (PEM)-West B mission [Hoell et al., 1997] and found that Asian fossil fuel+biomass burning emissions led to gross photochemical formation of 18.9 Gmol/day within the

Asian boundary layer (0-3km) with gross photochemical destruction and surface deposition of 6.4 Gmol/day and 4.2 Gmol/day, respectively.

From a meteorological perspective, East Asia is a preferred region for springtime lee cyclogenesis over the Mongolian Plateau and coastal cyclogenesis in the Sea of Japan and East China Sea [Chen et al., 1991]. During March 2001, synoptic storms formed within the TRACE-P domain on average every 4 days [Fuelberg et al., this issue]. Consequently, transport of East Asian emissions during TRACE-P was dominated by synoptic-scale frontal lifting of polluted continental boundary layer air in the warm sector of the developing cyclones [Jaffe et al., 1999; Kaneyasu et al., 2000; Bey et al., 2001b]. Frontal lifting is an effective means of transporting boundary layer air to the middle and upper troposphere, where strong winds can lead to long-range transport of the East Asian emissions. Tropopause folds, which can bring stratospheric air deep into the free troposphere, are also associated with rapidly developing cyclones and upper-level frontogeneous [Lamarque and Hess, 1994].

The subtropical jet stream, with 200mb wind speeds of greater than 75 m/s in the jet core, determines middle and upper tropospheric winds over East Asia during March (Figure 1). This jet stream, often referred to as the "Japan Jet", is located in the axis the large-scale upper tropospheric climatological trough (Figure 1). The southern flank of this large-scale trough is a preferred region for stratosphere-troposphere exchange (STE) in the northern hemisphere winter [Hoerling et al., 1993]. The "tropopause break", defined as a break in the altitude of the tropopause or narrow region of indistinct tropopause [Palmen and Newton, 1969], is located to the south of this trough, coincident with the subtropical jet stream. Isentropic surfaces between approximately 380K and 320K intersect the tropopause break and connect the lowermost extratropical stratosphere to the subtropical troposphere [Holton et al., 1995]. Quasi-horizontal isentropic motion across the tropopause break can lead to STE [Folkins and Appenzeller, 1996]. Seo and Bowman [2001] found that globally, the largest stratosphere to troposphere fluxes occurred in northern hemisphere spring near 30^{o}N off the coast of East Asia. This isentropic STE is controlled by Rossby wave breaking along the subtropical jet and is consistent with the climatology of Rossby wave breaking on the 350K isentrope [Postel and Hitchman, 1999].

In-situ ozone production, strong STE, and rapid frontal lifting and tropopause folding due to frequent cyclogenesis result in a complex and rapidly evolving East Asian tropospheric ozone distribution during northern hemisphere springtime, complicating the diagnosis of an ozone budget for this region. In the current study we use the Regional Air Quality Modeling System (RAQMS), which was jointly developed by the NASA Langley Research Center (LaRC) and University of Wisconsin-Madison (UW), to estimate the ozone budget over East Asia during TRACE-P.

The paper is organized as follows. Section 2 describes the RAQMS model. Section 3 presents a discussion of the method used for estimating STE during TRACE-P. Section 4 describes the RAQMS TRACE-P simulation and compares the predictions with satellite and in situ observations as well as box-model estimates of ozone photochemistry to assess the fidelity of the simulations. Section 5 presents results from the STE calculations and section 6 discusses the East Asian tropospheric ozone budget analysis. Discussion and Conclusions are presented in Section 7.

2. RAQMS Model Description

RAQMS is a multi-scale meteorological and chemical modeling system for predicting stratospheric and tropospheric chemistry. RAQMS combines two meteorological forecast models (regional domain nested within a global domain) developed at UW with a stratospheric-tropospheric chemical prediction scheme that was developed at LaRC. The nesting is one-way, with chemical predictions from the global component ($RAQMS_G$) providing boundary conditions for a higher resolution nested component ($RAQMS_N$). During TRACE-P, $RAQMS_G$ was run using a 2^ox2^o latitude-longitude resolution and $RAQMS_N$ was run using a rotated equidistant projection centered at 26.5^oN and 115.0^oE with 110km horizontal resolution (60 grid points in east-west direction and 45 grid points in north-south direction). The TRACE-P $RAQMS_N$ domain is shown in Figure 1 and includes most of Eastern and Central Asia. The southern and western boundaries of the domain were chosen to include the primary biomass burning emission sources in S. E. Asia and the northern and eastern boundaries where chosen to capture the full extent of TRACE-P flight tracks. The RAQMS chemical predictions are conducted online using instantaneous meteorological conditions to

accurately account for large-scale advective processes and the exchange of trace gases via moist convection and boundary layer turbulence.

The $RAQMS_G$ meteorological prediction model is based on a vertical coordinate that smoothly transitions from terrain-following at the earth's surface to isentropic in the middle to upper troposphere (UW θ–η model). Numerical integration in isentropic coordinates provides decided advantages for simulation of the long-range transport of atmospheric properties [Johnson et al., 1993, 2000, 2002; Zapotocny et al., 1997a,b]. These advantages are most pronounced in baroclinic regimes, where transport is primarily two-dimensional in isentropic coordinates and errors related to vertical advection are negligible. This simplification translates to improved simulation of atmospheric transport of conservative tracers [Zapotocny et al., 1996, 1997a,b]. The UW θ–η model was developed through modification of the UW hybrid isentropic-sigma (θ–σ) coordinate model [Zapotocny et al., 1994, 1996, 1997a,b; Johnson et al., 2000, 2002] and employs flux form piecewise parabolic method (PPM) numerics [Colella and Woodward, 1984; Carpenter et al., 1990] on the Arakawa A grid. The PPM scheme is highly accurate both in the vicinity of sharp gradients and for smooth flows [Carpenter et al. 1990]. The monotonicity constraint employed frees the solutions from spurious oscillations, and fields such as water vapor, chemical species, and mass within isentropic layers remain positive definite during integration. The UW θ–η model incorporates the full suite of the National Center for Atmospheric Research (NCAR) Community Climate Model 3 (CCM3) physical parameterizations including radiation, moist convection, vertical diffusion, gravity wave drag, Planetary Boundary Layer (PBL) scheme, and surface fluxes. Kiehl et al. [1996, 1998] provide a detailed description of the physical parameterizations employed in CCM3. Vertical mixing due to non-local atmospheric boundary layer turbulence [Holtslag and Boville, 1993] and mass-flux convection [Zhang and McFarlane, 1995] are applied to the transported chemical species.

The $RAQMS_N$ meteorological prediction model is the UW Non-hydrostatic Modeling System (UW-NMS) [Tripoli, 1992]. UW-NMS is a regional-scale non-hydrostatic numerical weather prediction model that can resolve atmospheric structure on spatial scales as low as 10 km in the horizontal and 200 - 400 m in the vertical. Advection is formulated using a 6th order Crowley scheme in flux form. Unresolved turbulent

exchange is represented using a modified 1.5 level Turbulent Kinetic Energy (TKE) closure and a modified Emanuel moist convection. The UW-NMS explicitly predicts distributions of cloud liquid water, pristine ice, rain, and snow. The UW-NMS has been applied to studies of tropical cloud clusters, hurricanes, mid-latitude cyclones, polar lows, and mesoscale convective systems [Pokrandt et al., 1996; Mecikalski and Tripoli, 1998; Avissar et al., 1998]. The model has been used to study the impact of synoptic waves on summer column ozone as part of the NASA Polar Ozone Loss over the Arctic Region in Summer (POLARIS) aircraft campaign [Hitchman et al., 1999] and the impact of inertial gravity waves on polar stratospheric clouds as part of the NASA SAGE III Ozone loss and Validation Experiment (SOLVE) campaign [Hitchman et al, 2003]. The UW-NMS can resolve mesoscale deformations of the tropopause associated with cut-off lows which can lead to irreversible STE.

For the TRACE-P simulations $RAQMS_G$ extends up to approximately 60km with a full representation of stratospheric dynamics and chemistry. There are 26 $\theta-\eta$ levels in the vertical: 12 η levels that transition from sigma coordinates at the surface to isentropic coordinates at η_θ= 336K (near the mid-latitude tropopause) and then 14 isentropic layers up to 3300K (upper stratosphere). Five η layers are below 800mb. The $RAQMS_N$ domain uses 50 altitude levels with a fixed vertical resolution of 400m from the surface to 20km, allowing the influence of STE processes on East Asian tropospheric ozone distributions to be accurately assessed.

The RAQMS global and regional models use an identical chemistry module that includes standard stratospheric odd oxygen (O_x), hydrogen oxide (HO_x), nitrogen oxide (NO_x), chlorine oxide (ClO_x), and bromine oxide (BrO_x) reactions, tropospheric NO_x-HO_x reactions, and oxidation of methane (CH_4) and carbon monoxide (CO). Non-methane hydrocarbon (NMHC) chemistry is not implemented in the version of the module described here. The chemistry module is based on the LaRC Interactive Modeling Project for Atmospheric Chemistry and Transport (IMPACT) model [Eckman et al., 1995; Pierce et al., 2000; Al-Saadi et al., 2001]. The chemistry computes concentrations for 53 species (Table 1) using 41 photolytic and 101 gas-phase reactions. Thirty-six chemical families and species are explicitly transported (Table 2), including total odd oxygen, total odd nitrogen, and total inorganic chlorine and bromine.

Kinetic rates and photolytic quantum yields and absorption cross sections are from DeMore et al. [1997] and Sander et al. [2000]. The photolytic rates are based on normalized radiative flux functions tabulated as a function of solar zenith angle, overhead column ozone, wavelength, and temperature [S.R. Kawa, private communication, 1996]. For photolysis, a surface albedo of 10% is assumed in the troposphere and a global albedo of 30% is assumed for the stratosphere (to account for underlying tropospheric cloud effects). Surface deposition is computed according to the surface type and drag coefficient, with the calculation of the deposition destruction rate modeled after Galbally and Roy [1980] and Levy et al. [1985]. Dry deposition is computed for ozone (O_3), peroxides, aldehydes, nitrogen dioxide (NO_2), CO and nitric acid (HNO_3) using deposition velocities from Muller and Brasseur [1995]. Rainout is based on first order rate constants that are fixed in the troposphere. Additionally, heterogeneous loss of nitric pentoxide (N_2O_5) is based on zonal averaged rates from Dentener and Crutzen [1993].

An updated CO emission inventory was developed for the TRACE-P simulations [Kiley et al., this issue]. This $1^o x 1^o$ source combines global monthly biomass burning CO emissions [Duncan et al., 2002] and global annual industrial emissions derived at Harvard University [J.A. Logan, personal communication, 2002] with 2000 estimates of industrial and biofuel emissions over East Asia [Streets et al., this issue]. Additional global sources of CO in RAQMS include an oceanic source equal to 40 Tg/year and estimated sources from isoprene and terpene oxidation based on the Global Emissions Inventory Activity (GEIA) Emission Database for Global Atmospheric Research (EDGAR) database. Production of 2.5 moles of CO per mole of isoprene and 0.8 moles of CO per mole of monoterpenes are assumed. These assumptions result in global CO sources of 585 Tg/year from isoprene and 24 Tg/year from terpenes. The total global CO emissions are 1571 Tg/year. Industrial NO_x emissions are from the $1^o x 1^o$ GEIA/EDGAR emission inventory, with East Asian emissions replaced by those from Streets et al. [this issue]. Aircraft NO_x emissions are obtained from the NASA High Speed Research Program (HSRP) data base [Stolarski et al., 1995] and lightning emissions are distributed according to Price et al. [1997] with an annual source of 3 Tg of nitrogen. Monthly NO_x emissions from soils are based on Yienger and Levy [1995], as in the GEIA/EDGAR database. Biomass burning emissions of NO_x are scaled to those of CO. The $1^o x 1^o$

inventories are mapped onto the grids used within the RAQMS regional and global models. Surface sources of nitrous oxide (N_2O), CH_4, and halocarbons are implicitly assumed by imposing a constant mixing ratio at the surface appropriate for 1990 [WMO, 1993].

The RAQMS stratospheric chemistry has been extensively evaluated through comparisons with in-situ stratospheric measurements [Pierce et al., 1997, 1999, 2002] and with stratospheric satellite climatologies [Al-Saadi et al., 2001]. For evaluation of tropospheric chemistry, monthly mean chemical climatologies from a multi-year IMPACT model simulation using identical chemistry and emissions databases to RAQMS were examined (not shown). Climatological seasonal variations of ozone at mid-latitude ozoneonde stations show good agreement with ozoneonde data throughout the troposphere, but the model underestimates the observed ozone mixing ratios at tropical ozoneonde stations. Seasonal variations in surface CO are in agreement with climatological data from the National Oceanic and Atmospheric Administration (NOAA) Climate Modeling and Diagnostics Laboratory (CMDL). Additionally, comparisons between climatological altitude profiles of O_3, CO, HNO_3, NO_x, hydrogen peroxide (H_2O_2) and methyl hydroperoxide (CH_3OOH) were compared to composite profiles from various GTE field campaigns (PEM West-A, PEM West-B, PEM Tropics-A, PEM Tropics-B and TRACE-A [Emmons et al., 2000]). The comparisons showed that the IMPACT climatological profiles capture the main features (vertical and latitudinal structure) of the field campaign composites.

3. Method for estimating STE

The East Asian tropospheric ozone budget during TRACE-P is computed using the $RAQMS_N$ regional domain to define the lateral boundaries of the budget calculations. The tropospheric ozone budget within the $RAQMS_N$ domain is determined by the balance between the following physical processes: horizontal fluxes of ozone through the western, northern, eastern, and southern boundaries of the domain, net in situ tropospheric photochemical production (gross formation – gross destruction), surface deposition, vertical fluxes across the tropopause, and movement of the tropopause. This section outlines the procedure for determining the STE component of the tropospheric ozone budget for East Asia.

Numerous approaches for estimating the flux of mass and trace gases through the tropopause have been developed. Holton et al. [1995] provide an overview of these approaches. Most model-based approaches rely on a variant of the generalized formulation discussed by Wei [1987] using either a thermal or dynamical definition of the tropopause. Hoerling et al. [1993] conducted a global analysis of STE during January using Wei's isentropic formulation and both dynamical and thermal tropopause definitions. Dynamical and thermal definitions of the tropopause produced similar results although the downward mass flux was somewhat larger across the thermal tropopause than the dynamical tropopause. Wirth and Egger [1999] compared 5 methods of diagnosing the synoptic scale STE including trajectory based estimates (which determine mass flux using kinematic trajectories to define a center of mass for a finite volume), variations of Wei's general formulation, and a direct approach. They found that Wei's generalized formula produced different results depending on which coordinate system was used due to near cancellation of large opposing terms. Using potential vorticity (PV) as both a vertical coordinate and tropopause definition provided the most realistic STE for the case considered but required detailed knowledge of the three-dimensional time variation of sources and sinks of PV. A direct method, based on approximating the tropopause using two triangles for each grid box, showed similar grid scale features as the Wei approach in both pressure and potential temperature.

The proximity of the subtropical jet and associated tropopause break complicates the calculation of STE during TRACE-P for a number of reasons. First, the domain of interest extends from approximately 45^{o}N to the equator (Figure 1). Dynamical definitions of the tropopause are only appropriate in mid-latitudes. Because of this, we chose the thermal definition of the tropopause for our STE calculations. Second, the tropopause break leads to first order discontinuities in pressure, altitude and potential temperature on the tropopause. Gradients of these quantities along the tropopause determine the horizontal component of STE in Wei formulations, and sharp discontinuities lead to large numerical errors. Third, mass flux estimates based on trajectory based techniques suffer from the effects of strong shear deformation within the subtropical jet. Initially compact volume elements are elongated along the jet axis, so that the position of a single trajectory cannot be used to define its center of mass. Based on

these considerations, we have chosen a direct approach for evaluating STE within the $RAQMS_N$ domain. Following Wirth and Egger [1999], the cross-tropopause mass flux $F(\rho)$, expressed as a flux per unit horizontal area, is given by

$$F(\rho) = (\rho(\mathbf{u}-\mathbf{c}_{tp})\cdot\mathbf{n})/\cos(\alpha) \quad (1)$$

Where ρ is density, $\mathbf{n}$ is the upward normal vector to the tropopause, $\mathbf{u}$ is the 3-dimensional velocity vector, $\mathbf{c}_{tp}$ is the vector defining the motion of the tropopause (in direction of unit normal), and α is the angle between $\mathbf{n}$ and the vertical (equation 4 in Wirth and Egger [1999]). The magnitude of $\mathbf{c}_{tp}$ is given by

$$|\mathbf{c}_{tp}| = \cos(\alpha)|\delta z^{tp}/\delta t| \quad (2)$$

Where z^{tp} is the altitude of the tropopause. Wirth and Egger [1999] defined the local tropopause based on triangles; we consider a discrete thermal tropopause defined by the faces of the $RAQMS_N$ grid boxes and then compute fluxes across those horizontal and vertical faces separating the troposphere from the stratosphere.

Figure 2 is a schematic illustration of the discrete flux calculation. The discrete tropopause (bold line) is represented by a series of stair-step increments. $RAQMS_N$ uses an Arakawa C-grid, consequently O_3 mixing ratios are defined at the center of each box, horizontal velocities are defined on the vertical faces, and vertical velocities are defined on the horizontal faces. The schematic illustrates a case where the tropopause break spans more than one vertical grid-box. In these instances, the flux normal to the tropopause surface (indicated by the dashed line), for the grid boxes in column (i) are determined by 1) integrating the zonal and meridional fluxes over the local depth of the tropopause break, 2) projecting this flux onto the horizontal plane, 3) adding the vertical fluxes associated with the upper tropospheric box in column (i), and 4) adding the horizontal projection of the flux associated with the local movement of the tropopause $\mathbf{c}_{tp}$ for the upper tropospheric grid box in column (i).

The horizontal projection of the flux due to the movement of the tropopause is determined by substitution of equation (2) into equation (1) which results in cancellation of the $\cos(\alpha)$ term in the evaluation the horizontal projection of $\mathbf{c}_{tp}$. The O_3 flux is obtained by multiplying $F(\rho)$ by ozone number density at the discrete tropopause, which is obtained by averaging ozone number densities in adjacent grid boxes.

4. RAQMS TRACE-P Simulations

The $RAQMS_G$ predictions were conducted from February 15th to April 15th, 2001 and were constrained with assimilated meteorological data from the European Center for Medium range Weather Forecasting (ECMWF) $1^o x 1^o$ analysis. The $RAQMS_N$ prediction was conducted from March 7th to April 12th, 2001 using 6 hour meteorological fields from the NOAA National Centers for Environmental Prediction (NCEP) Aviation Model (AVN) $1^o x 1^o$ degree analysis for lateral boundary conditions. Meteorological fields from the AVN assimilation were used in the regional simulation because of problems encountered with orographically locked vertical velocities in regional forecasts using ECMWF analyses. These vertical velocities resulted in unrealistic ozone fluxes at the tropopause. Initial chemical conditions for the global simulation were obtained from February monthly means from a multi-year coupled chemical climate run with the LaRC IMPACT model. Initial and boundary conditions for the chemical constituents in regional predictions were obtained from the $RAQMS_G$ prediction.

$RAQMS_G$ was run for a series of 6hr forecast cycles. At the end of each 6hr forecast the meteorological variables were re-initialized with ECMWF assimilated fields and the predicted chemical distributions were carried forward. $RAQMS_N$ potential temperature and water vapor predictions were relaxed towards the AVN assimilated fields to provide a weak constraint on the regional meteorological forecasts. These procedures result in online global and regional chemical simulations that closely track the synoptic evolution within the assimilated meteorological data sets.

4.1 Large-scale Ozone Distribution during TRACEP

This section presents comparisons between the RAQMS predictions and satellite and aircraft remote measurements to demonstrate the model's ability to predict stratospheric and tropospheric ozone distributions over a wide range of spatial and temporal scales. The discussion highlights the multi-scale aspects of the RAQMS prediction and establishes the fidelity of the RAQMS TRACE-P simulations. Figure 3 shows observed and predicted March mean total column ozone, tropospheric column ozone, and composite ozone cross sections. The largest total column ozone amounts (left panels in Figure 3) are found in Northern Hemisphere high latitudes. The Southern Hemisphere shows much lower column ozone. These hemispheric asymmetries are

captured in the $RAQMS_G$ column ozone, although the predicted column is overestimated by approximately 50DU over the North Pole and is lower than TOMS in the tropics. This overestimate at the North Pole and underestimate in the tropics is consistent with an overly strong stratospheric Brewer-Dobson circulation in the ECMWF analysis, a feature found in many data assimilation systems [Huesmann and Hitchman, 2003], although the overestimate at the North Pole could also be due to neglecting heterogeneous chemistry associated with polar stratospheric clouds (PSCs) in the TRACE-P simulation. As shown below, the higher observed tropical column ozone could be influenced by tropical tropospheric ozone production due to biomass burning in South America and Central Africa during March 2001.

Large-scale upper tropospheric circulation patterns play an important role in determining the longitudinal variations in the altitude of the tropopause and hence column ozone. In regions that are dominated by climatological high-pressure systems, such as over central Asia and the eastern Pacific, the tropopause is elevated and there is a clear latitudinal separation between the high northern latitude and low tropical column ozone. In regions that are dominated by climatological low-pressure systems, such as over the eastern coasts of Asia and North America, the transition from high extra-tropical and low tropical column ozone is very sharp, with column ozone dropping from 450DU to 250DU over East Asia near 30^oN. The predicted column ozone is in good agreement with the observed distribution in the East Asian region, indicating that the important features of both the large-scale lower stratospheric ozone transport and tropopause pressures are being accurately predicted within $RAQMS_G$ model. This is critical for the RAQMS predictions of tropospheric ozone formation and destruction during TRACE-P since the sharp gradient in springtime column ozone at 30^oN leads to large changes in photolysis rates over East Asia which play a critical role in tropospheric photochemistry in this region [Crawford et al., 1997].

To compare the observed and predicted tropospheric column ozone we use daily TOMS/SBUV derived TOR data from Fishman and Balok [1999]. We sampled daily $RAQMS_G$ tropospheric column ozone (TCO, analogous to the satellite-derived TOR) at the locations of TOMS/SBUV TOR and then averaged those daily distributions from March 1-25^{th} (the last day with TOR estimates). The observed TOR is obtained by

subtracting 5-day averaged stratospheric columns derived from empirically corrected SBUV observations from daily TOMS columns [Fishman and Balok, 1999]. At middle latitudes, 5-day averaging of the SBUV observations leads to smoothing of the lower stratospheric signatures of tropospheric synoptic disturbances in the column ozone, which often results in aliasing of the synoptic features when subtracted from TOMS. This artifact is similar to one described by Fishman et al. [1990] when SAGE (Stratospheric Aerosol and Gas Experiment) data were used with TOMS to calculate the residual. To minimize the effects of this aliasing the objective screening of the TOR data described in Fishman et al. [1990] was used except we relaxed the TOR <60DU restriction to allow for the possibility of higher TOR. We have attempted to assess the degree of synoptic aliasing using a daily noise index defined as the fraction of TOR estimates less than 10DU within a latitude band. Latitudes with time averaged noise levels greater than 10% were excluded. Points with March 1-25 sampling of less than 66% were also excluded. The observed daily TOR was also filtered in longitude with a 10-point (12.5^{o}) running mean filter to reduce the influence of scan angle dependent biases in the TOMS data.

Both the observed TOR and predicted TCO distributions (middle panels in Figure 3) are dominated by a 40-50DU maximum that generally coincides with the northern hemisphere subtropical gradient in the tropopause pressure during March 2001. The predicted and observed distributions are in good agreement within the high-pressure circulation in the eastern Pacific, but in general the predicted northern hemisphere subtropical TCO is higher than the observed TOR. The predicted East Asian TCO shows a broad maximum extending over the Western Pacific while the observed East Asian TOR is significantly lower. Both observed and predicted TOR fields show a dominant wave-one pattern in the tropical latitudes with a broad minimum over the Pacific basin. This pattern is partially driven by the zonal Walker Circulation with ascending motion associated with convection over Indonesia leading to low tropospheric columns and descending motion over the equatorial Atlantic leading to higher tropospheric columns. However, the observed TOR shows enhanced tropospheric ozone over Brazil and Central Africa, presumably associated with biomass burning in this region. These features are absent in the predicted TCO due to the neglect of NMHC chemistry and lack of significant biomass burning emissions in the model's climatological emission data bases

during March in these regions. The additional ozone formation associated with biomass burning increases the amplitude of the wave-one tropical feature in the observed TOR. The predicted band of elevated tropospheric ozone near 30°S is in good agreement with observations.

The right panels in Figure 3 show comparisons between East Asian ozone composite cross-sections obtained by the Ultra-Violet Differential Absorption Lidar (UV DIAL) instrument [Browell et al., this issue] and $RAQMS_N$ predictions (sampled at the DIAL measurement locations). The $RAQMS_N$ prediction shows evidence of the convective lifting signatures observed in the tropical upper troposphere although the predicted mixing ratios are not as low as observed. This may be due to lateral mixing of high ozone amounts predicted at 25°-30°N near 15km that are overestimated in the model. Both observed and predicted tropospheric ozone mixing ratios exceed 100ppbv below the thermal tropopause from 30°-45°N, consistent with the predicted high East Asian TCO at these latitudes. Observed and predicted ozone mixing ratios in excess of 60ppbv extend down from the tropopause to 5km at 25°N, suggesting that STE plays a significant role in determining the airmass characteristics in this region. DIAL airmass characterization [Browell et al., this issue] indicates that approximately 35% of the DIAL ozone observations north of 25°N were associated with stratospheric air. $RAQMS_N$ underestimates mid tropospheric ozone mixing ratios between 40° and 45°N. However, this latitude band was sampled by only one DC8 flight (figure 1).

To quantify the differences between RAQMS ozone predictions and observations we compared longitudinally averaged column ozone distributions. Figure 4 shows the results of these comparisons. The upper panel shows that the $RAQMS_G$ zonal total mean column ozone is within 10-20DU of the TOMS observations except poleward of 70°N, where $RAQMS_G$ column ozone is high by as much as 50DU. The middle panel shows that $RAQMS_G$ TCO predictions underestimate the zonal mean observed TOR by 10DU at 10°S and overestimate the zonal mean observed TOR by 10DU at 25°N. As discussed above, the model underestimate at southern low latitudes is primarily a result of using climatological biomass burning estimates and neglecting NMHC chemistry.

The lower panel shows latitudinal distributions of East Asian TOR from TOMS/SBUV, $RAQMS_G$ TCO, and $RAQMS_N$ TCO averaged between 120°-150°E (the

longitudinal extent of the TRACE-P DC8 flights), as well as the TCO obtained from the DIAL and DIAL-sampled $RAQMS_N$ composites. The DIAL composite TCO provides an independent measure of the tropospheric column ozone for interpretation of the differences between the RAQMS predictions and TOMS/SBUV observations in E. Asia. Furthermore, comparisons between the $RAQMS_N$ predictions averaged between 120^o-150^oE and the DIAL-sampled $RAQMS_N$ composite provide a measure of biases introduced in the DIAL composite TCO by the DC8 flight sampling.

Overall, the East Asian comparisons show that 1) The East Asian $RAQMS_N$, $RAQMS_G$, and TOMS/SBUV TOR are within 5-10DU of each other in the tropics and subtropics (0^o-20^oN), 2) The East Asian DIAL-sampled $RAQMS_N$, $RAQMS_G$, and DIAL composite TCO are within 5-10DU of each other on the equatorward flank of the Japan Jet (20^o-30^oN) (the high bias in $RAQMS_N$ is associated with overestimates in ozone mixing ratios just below the tropopause), 3) TOMS/SBUV underestimates the TOR within the Japan Jet (30^oN) by 10-15DU relative to the DIAL composite, 4) The DIAL-sampled $RAQMS_N$ prediction is in good agreement with the DIAL composite on the poleward flank of the Japan Jet (30^o-35^oN), and 5) Comparison of the DIAL-sampled and $RAQMS_N$ predictions averaged between 120^o-150^oE shows that DC8 flight sampling captures the time averaged TCO except within (+/-) 4^o of the Japan Jet (30^oN), where DC8 sampling underestimates of the time averaged TCO by up to 10DU.

The $RAQMS_N$ predictions averaged between 120^o-150^oE shows time averaged East Asian TCO of 60DU at 35^oN, nearly 20DU higher than the $RAQMS_G$ predictions and 25DU higher than the TOMS/SBUV TOR at this latitude. The good agreement (differences <5DU) between the DIAL-sampled $RAQMS_N$ and the DIAL composite TCO at these latitudes provides confidence that the $RAQMS_N$ TCO prediction is realistic and points to a low bias in both the $RAQMS_G$ TCO and TOMS/SBUV TOR within the Japan Jet. Slightly different averaging periods could account for some of these differences. However, we attribute the low bias in the $RAQMS_G$ prediction primarily to the relatively coarse horizontal resolution (2^ox2^o) in the global simulation (the global and regional vertical resolutions are similar in the lower stratosphere).

The inability of the TOMS/SBUV data to capture the increase in TCO within the Japan Jet is most likely related to the algorithm used to extract upper tropospheric and

lower stratospheric information from the relatively low vertical resolution SBUV measurements. The SBUV profile inversion is done in 12 Umkehr layers with the lowest layer (1013-253 mb) nearly 12 km thick. As a result, all of the lowest layer in the SBUV retrieval is assumed to be tropospheric [Bhartia et al., 1996], whereas in reality, some of this layer contains stratospheric air (especially during times of active stratosphere-troposphere exchange) which is not being subtracted from the SBUV total column ozone. The net effect of this assumption is that the resultant stratospheric column ozone (SCO) integral is overestimated. Consequently, when the SCO is subtracted from the concurrent TOMS total ozone measurement, the difference (TOR) is too low. Fishman and Balok [1999], developed a procedure that uses the ozoneonde climatology from Logan [1999] to empirically correct the SBUV profile in the lowest three Umkehr layers. During this specific case study, this climatology does not capture the high ozone mixing ratios found below the thermal tropopause within the neighborhood of the Japan Jet (see Figure 3), and consequently too much ozone is placed in the stratospheric part of Umkehr layer 2. When the SBUV stratospheric column is subtracted from the TOMS total column, this partitioning leads to the low TOMS/SBUV TOR.

4.2 March 17, 2001 Case Study

It is clear from the previous discussion that the tropopause break and subtropical jet play a significant role in determining the upper tropospheric O_3 distribution off the coast of East Asia. This is illustrated by considering a case study for DC8 flight 11, which occurred on March 17, 2001. The upper left panel of Figure 5 shows the TOMS column ozone, tropopause pressures, and flight track for DC8 flight 11. The flight originated from Hong Kong, traversed a cold front, and then returned westward before descent into Okinawa, Japan. The tropopause break is evident in the sharp gradient in tropopause pressures near 30^{o}-35^{o}N that extends across southern Japan. The northernmost leg of the flight track (indicated by thick red line) is the focus of this case study. This flight leg lies near 30^{o}N and extends from 131^{o}-138^{o}E, roughly parallel to the tropopause break. The tropopause pressure increases (and tropopause altitude decreases) rapidly directly north of this flight segment with tropopause pressures increasing from 140mb to 220mb across the break at these longitudes. TOMS total column ozone ranges from 350-450 DU to the north and 250-300 DU to the south of the break.

DIAL ozone measurements (upper right panel of figure 5) show that tropospheric ozone mixing ratios are generally between 20 and 40 ppbv except for a thin layer near 8km with mixing ratios ranging from 40-100ppbv. The tropical tropopause is clearly evident at 17-18km where ozone mixing ratios increase to >100ppbv. From 06-08Z (indicated in red along the flight track) the DC8 encountered a much deeper layer of high ozone mixing ratios (>80ppbv) near 6km. A north-south cross section (nearly perpendicular to the flight track) through this feature from the $RAQMS_N$ prediction (lower left panel of figure 5) shows that the subtropical jet stream defines an airmass boundary between tropical upper tropospheric air and mid-latitude lower stratospheric air. To the south, ozone mixing ratios are near 40ppbv in the tropical upper troposphere while to the north ozone mixing ratios are in excess of 100ppbv in the mid-latitude lower stratosphere. The tropopause break extends from 10-16km on the northern flank of the subtropical jet. The mismatch between the thermal and chemical characteristics of the air between the subtropical jet core and the tropopause break results in stratospheric air (from a chemical point of view) below the thermal tropopause. The high ozone within this airmass contributes to the high TCO that RAQMS predicts near 30^{o}N over East Asia (Figure 3). An upper tropospheric front is evident in the vertically compact isentropes below the jet maximum. Ozone mixing ratios in excess of 100ppbv extend southward from the tropopause break down to 5km along this upper level front. The high ozone in the DIAL curtain between 06-08Z (this segment of flight track is colored in red) corresponds to the southern extent of this tongue of high ozone. Similar tongues of high ozone were observed on many of the TRACE-P flights and account for the high ozone north of 25^{o}N that is found in the observed and predicted composite cross-sections shown in Figure 3.

The lower right panel of Figure 5 shows a comparison between the $RAQMS_N$ prediction and in situ O_3 measurements [Avery et al., 2001]. The DC8 sampled the layer of elevated ozone on each of the flight legs above 5km. The model predicts a relatively uniform layer with ozone mixing ratios near 50ppbv prior to 06Z while in situ measurements show a complex structure within the layer with mixing ratios ranging from 20-80ppbv. The model prediction of mixing ratios within the tongue of high ozone

encountered between 06Z and 08Z is in good agreement with the in situ measurements with peak ozone mixing ratios over 100ppbv and levels above 60ppbv down to 3km.

4.3 Statistical comparison with in situ measurements

The preceding discussion demonstrates that the RAQMS predictions are able to reproduce the time averaged ozone distributions observed during TRACE-P and represent the STE transport processes which give rise to a significant portion of the observed ozone distributions in the upper troposphere. However, using RAQMS to diagnose the O_3 budget during TRACE-P also requires accurate assessment of the photochemical formation and destruction within the TRACE-P domain. The ability of the RAQMS O_3 predictions to capture daily variations in ozone transport, STE and in-situ photochemical processes was assessed by statistical comparison with 1-minute averaged in situ O_3 and NO_x [Koike et al., this issue] from the DC8 and P3B aircraft measurements. For a comparison of the $RAQMS_N$ and $RAQMS_G$ CO predictions with in situ measurements and other chemical forecast models that were involved in TRACE-P see Kiley et al. [this issue]. Additionally, predicted photochemical O_3 formation and destruction was compared to that calculated by a detailed photochemical time-dependent box model [Crawford et al., 1999]. The box model calculations also used 1-minute averaged data (referred to as the "merged" data set for TRACE-P and available on the GTE TRACE-P public data archive http://www-gte.larc.nasa.gov). Each point was run to diurnal steady state with long-lived species constrained to observations, and daily averaged O_3 production and destruction was then computed using the resulting theoretical radical predictions. This comparison includes only the East Asian flights during TRACE-P (DC8 flights 8-17 and P3B flights 8-20). RAQMS model results were temporally and spatially interpolated from 6-hour model output to the aircraft flight tracks for direct comparison to the observations and box model output.

Figure 6 shows the results of our statistical analysis. $RAQMS_N$ O_3 predictions (upper left) capture the observed median and variability in the 10-12km altitude range (note that the upper 90% percent have been truncated) but overestimates median ozone mixing ratios and variability between 8-4km. $RAQMS_N$ underestimates the median ozone mixing ratios below 2km by about 5-10 ppbv. This is consistent with the composite comparisons with DIAL measurements shown in Figure 3.

$RAQMS_N$ is in good agreement with median observed NO_x (upper right) except for a factor of 2 overestimate between 4-6 km. Median NO_x in the lowest km is overestimated by $RAQMS_N$ by approximately 20%. $RAQMS_N$ NO_x variability is lower than observed in the free troposphere, due to frequent plume encounters by the P3B and DC8 aircraft. High NO_x within the plumes increases the observed variability but cannot be resolved by the 110km grid used in the regional predictions. Diurnally averaged gross photochemical O_3 formation (lower left) and destruction (lower right) are in good general agreement with box model predictions constrained by in situ measurements although the $RAQMS_N$ formation rates are overestimated in the lowest km by nearly 40%. This overestimate of O_3 gross formation in the lowest km is consistent with corresponding overestimates of NO_x, and reflects the strong dependence of ozone formation on NO_x abundances. Note that although the predicted median gross destruction is in good agreement with box model estimates throughout the troposphere the low $RAQMS_N$ O_3 concentrations in the lowest 1km imply that the gross loss frequency for O_3 at this altitude is on the order of 20% higher than the box model.

$RAQMS_N$ ozone mixing ratios are lower than observed in the lowest 1km although the predicted median diurnally averaged net ozone production (gross formation - gross destruction) is slightly larger than predicted by the box model. There are several potential explanations for this. One is that surface deposition in RAQMS is too high. As will be shown later, loss due to surface deposition is 37% of the gross formation within the TRACE-P regional domain. Another explanation for the underestimate in ozone within the lowest km is that RAQMS is not simulating vigorous urban O_3 production and subsequent transport. Carmichael et al. [this issue] find that air masses originating from highly industrialized regions of East Asia (Tokyo, Seoul, Shanghai, coastal NE China) were NMHC limited. Urban O_3 production, occurring within air parcels prior to sampling by the aircraft, is likely underestimated in the current simulations since RAQMS does not include NMHC chemistry and has horizontal resolution that is too coarse to adequately simulate urban scale chemistry.

5. RAQMS estimates of STE

Figure 7 shows the zonal averaged flux of O_3 across the tropopause within the $RAQMS_N$ model domain for the period from March 07 –April 12, 2001. The components

of the O_3 flux and zonal averaged tropopause altitude are also shown. Negatives correspond to fluxes from the stratosphere to the troposphere. The total O_3 flux is into the troposphere except for a small flux (1-2x10^{11} mol/cm^2/sec) into the stratosphere on the equatorward side of the time averaged tropopause break. The stratosphere to troposphere flux reaches a maximum of –10x10^{11} mol/cm^2/sec (3.2 D.U./day) near 30°-35°N and is dominated by the vertical flux component. Horizontal fluxes result in net fluxes of ozone from the troposphere to the stratosphere. The movement of the tropopause results in net fluxes from the stratosphere to troposphere. These results are in agreement with vertical flux estimates at 7km over East Asia by Carmichael et al. [1998] for the period from May 1-15 1987. They found downward average fluxes of –6.7x10^{11} mol/cm^2/sec over the Sea of Japan north of 30°N and upward average fluxes of 1.7x10^{11} mol/cm^2/sec over the southern part of their East Asian domain (over the Pacific ocean).

The distribution of horizontal and vertical fluxes across the tropopause is consistent with the thermally direct transverse circulation [Bjerknes, 1951] in the entrance region of the Japan Jet, located just below the tropopause and to the south of the tropopause break (c.f. figure 5). The transverse circulation results in upward motion to the south, poleward motion above, descending motion to the north, and equatorward motion below the jet. Sharp cross-tropopause O_3 gradients above the jet lead to net horizontal and vertical fluxes into the stratosphere in the upper southern quadrant of this circulation. Sharp mid-latitude cross-tropopause O_3 gradients lead to vertical fluxes into the troposphere in the poleward part of the transverse circulation. The daily mean latitude of the tropopause break varies from 30°N to 34°N within the $RAQMS_N$ domain, but shows little systematic change over the TRACE-P time period. However, the mean altitude of the tropopause north of the tropopause break rises from near 11km during early March to 12km by mid April within the $RAQMS_N$ domain. The rising mid-latitude tropopause is in response to seasonal warming of the mid-latitude troposphere and leads to fluxes of O_3 from the stratosphere to the troposphere within the $RAQMS_N$ domain during the TRACE-P time period.

6. TRACE-P O_3 budgets

The ozone budget for the East Asian region during the TRACE-P mission is estimated by summing instantaneous estimates of tropopause O_3 fluxes, horizontal O_3

fluxes of on each of the lateral boundaries, 6hr averaged O_3 gross formation-gross destruction (net production), and 6hr averaged O_3 surface deposition within the $RAQMS_N$ domain from March 07th to April 12th, 2001. Figure 8 shows time average results of these calculations. The time averaged zonal mean O_3 number density for the $RAQMS_N$ domain shows a local maximum of over $110x10^{10}$ mol/cm^3 between 20^o and 30^{o}N below 3 km which was not evident in the DIAL sampled $RAQMS_N$ ozone composite shown in figure 3. These differences arise due to using number density instead of mixing ratio and spatial and temporal sampling by the aircraft. The time averaged zonal mean O_3 production shows net production below 2km north of 10^{o}N with peaks of $25x10^5$ mol/cm^3/sec between 10^o and 20^{o}N (associated with biomass burning over Thailand) and $33x10^5$ mol/cm^3/sec at 34^{o}N (associated with industrial emissions from coastal China).

The O_3 flux at the western boundary shows inflow reaching over $-3.5x10^{15}$ mol/cm^2/sec near 30^{o}N at both 10km and 15km, just to the south of the tropopause break. The Tibetan Plateau defines the lower boundary for the flux calculations north of 30^{o}N. The O_3 flux at the eastern boundary shows maximum outflow in excess of $6.5x10^{15}$ mol/cm^2/sec near 30^{o}N from 10 to 12km, nearly twice the maximum inflow on the western boundary. This significant increase in O_3 flux is primarily due to the increased upper tropospheric wind speeds on the eastern boundary associated with the core of the Japan Jet (Figure 1). The large difference in the eastern and western fluxes is largely accounted for by net influx from the northern boundary, which shows maximum influx into the domain of over $-2.5x10^{15}$ mol/cm^2/sec near 110^{o}E and outflow reaching $1.5x10^{15}$ mol/cm^2/sec (east-west extent of the $RAQMS_N$ domain is 33% larger than the north-south extent). The inflow/outflow pattern on the northern boundary is determined by the location of the planetary scale trough (Figure 1), evident in the lower tropopause near 140^{o}E, with inflow upstream and outflow downstream of the trough. There are no significant fluxes on the southern boundary of the $RAQMS_N$ domain.

Figure 9 shows time series of spatially integrated contributions from the various components of the O_3 budget. In general, the large horizontal O_3 fluxes shown in Figure 8 tend to balance throughout the TRACE-P time period. Fluxes through the tropopause are predominately negative (into the domain) but there is a high degree of variability at both synoptic (2-3 day) and faster timescales. Surface deposition remains nearly constant due

to the use of climatological drag coefficients in the deposition velocity calculations. The net O_3 production reaches up to 1 Tg/day and shows a strong diurnal cycle with a longer period (~10day) modulation in peak production.

The total O_3 in the $RAQMS_N$ domain was initially 22.8 Tg. The lower left panel shows a time series of the actual accumulated (instantaneous-initial) O_3 along with the ozone accumulation predicted by our budget calculations (sum of the individual net tendencies). The predicted ozone accumulation when horizontal fluxes, STE or net production is excluded is also shown. The latter three time series illustrate the relative importance of these terms in the overall budget. There is little net change (final-initial) in the amount of ozone in the $RAQMS_N$ domain. The close agreement between the actual accumulated O_3 and the sum of our budget calculations indicates a high degree of accuracy in the budget calculations. The accumulated ozone within the $RAQMS_N$ domain is generally less than would be the case if the horizontal fluxes were ignored, reflecting net outflow, but neglecting the horizontal fluxes results in very small differences in the accumulated ozone by the end of the time period. On the other hand, neglecting either STE or net photochemical production results in significant declines in the ozone within the $RAQMS_N$ domain. By the end of the TRACE-P time period, STE has contributed 7 Tg, net in situ photochemical production has contributed 13 Tg, and surface deposition (not shown) has destroyed 20.75 Tg of O_3 over East Asia. However, the net photochemical production is itself a balance between gross formation and destruction. Gross formation produces 52 Tg, and gross destruction results in the loss of 39.25 Tg of O_3 over East Asia (not shown).

7. Discussion and Conclusions

A multi-scale modeling system that includes both stratospheric and tropospheric dynamical and chemical processes has been used to evaluate the East Asian ozone budget during TRACE-P. The computed ozone budget explicitly accounts for stratosphere troposphere exchange processes by computing the O_3 flux across a discrete tropopause defined by the model coordinate system. The $RAQMS_G$ total column ozone predictions compare favorably with TOMS measurements and possible reasons for differences between the $RAQMS_G$ TCO and SBUV/TOMS TOR within the TRACE-P domain have been identified. These analyses provide confidence that $RAQMS_G$ predictions can be

used as lateral boundary conditions for higher resolution $RAQMS_N$ predictions that focus on the East Asian region. The regional predictions are shown to be in good agreement with remote and in situ O_3 and NO_x measurements collected during TRACE-P. The predicted gross O_3 formation and destruction rates for air masses sampled by the DC8 and P3B are consistent with results from box model calculations that are constrained by in situ measurements and include much more detailed treatment of tropospheric chemical processes.

The overall fidelity of the TRACE-P simulations has allowed us to explicitly evaluate the East Asian tropospheric ozone budget. Table 3 summarizes the average O_3 budget during the period from March 07th to April 12th, 2001. The average predicted accumulation is 1.04 Tg and the average actual accumulation is 0.966 Tg, indicating an overall accuracy in the budget calculations of 7%. Gross formation (F) dominates STE by a ratio of 7 to 1 in East Asia during TRACE-P. However, this ratio is strongly influenced by the altitude of the tropopause. Sensitivity tests were conducted to examine this dependence. In these tests the instantaneous STE was computed across surfaces defined by the local tropopause minus 2km and minus 4km. The STE was reduced by 35% when the tropopause was lowered by 2km and by 28% when the tropopause was lowered by 4km. These sensitivity tests indicate that approximately 30% of the ozone advected from the stratosphere across the tropopause over East Asia is subsequently advected out over the Western Pacific within the upper 4km of the troposphere by the Japan jet.

The average net photochemical production (F-D) within the $RAQMS_N$ domain is 0.37 Tg/day, or 7% of the average eastward flux (5.25 Tg/day) during the TRACE-P time period. These results are consistent with Liu et al. [2002] who estimate eastward ozone fluxes from Asian fossil fuel and biomass burning account for 9.5% (0.575 Tg/day) of the total eastward flux (~6 Tg/day) between 1000-200mb and 10-60^{o}N at 150^{o}E during March. However, the present budget analysis implies a very close balance between sources and sinks (STE+F-D-Dep=0.043 Tg/day) within the $RAQMS_N$ domain during the TRACE-P time period. This balance results in very small average accumulation (~1 Tg) of O_3 in the East Asian region and very little export averaged over the period (0.03 Tg/day).

The low ozone export from East Asia predicted by $RAQMS_N$ during TRACE-P is a consequence of relatively high dry deposition rates. $RAQMS_N$ O_3 loss due to surface deposition is -0.546 Tg/day. Carmichael et al. [1998] estimate ~6.5 Tg O_3 was removed from their regional model domain during the period from May 1-15, 1987, corresponding to an average loss due to dry deposition of -0.433 Tg/day, or 20% lower than the current deposition rates. The $RAQMS_N$ dry deposition is 37% of the gross formation within the TRACE-P regional domain. This is consistent with the global ozone budget in the IMPACT model (with identical chemistry), which has globally averaged dry deposition rates of ~1235 Tg/yr, or 32% of the globally averaged formation rates. The 1235 Tg/yr global loss due to dry deposition in the IMPACT model is significantly higher than the 700 +/- 300 Tg/yr quoted by Lelieveld and Dentener [2000] but close to the GEOS-CHEM model global deposition of 1070 Tg/yr [Bey et al., 2001a]. However, both the IMPACT model and RAQMS have larger percentage contributions to the ozone budget from deposition than GEOS-CHEM due to lower gross formation rates. The 37% ratio of surface deposition to gross formation reported here is more than 50% higher than quoted by Bey et al. [2001b] who indicate that 21% of ozone produced within their Asian domain is lost to surface deposition, although this comparison is somewhat misleading since our surface deposition includes loss of non-Asian ozone while Bey et al. [2001b] are expressing their results relative to Asian ozone. The $RAQMS_N$ ozone budget predictions should be interpreted in light of these considerations. Finally, the influence of urban-scale ozone production on the East Asian ozone budget has not been accounted for in the RAQMS simulations and needs to be explored in more detail. These studies require higher resolution regional simulations and treatment of NMHC chemistry. A second generation RAQMS chemistry module, which includes treatment of NMHC species, has been developed and future studies will explore sensitivities to model resolution and chemical mechanisms.

References:

Al-Saadi, J. A., R. B. Pierce, T. D. Fairlie, M. M. Kleb, R. S. Eckman, W. L. Grose, M. Natarajan, J. R. Olson, Response of middle atmosphere chemistry and dynamics to volcanically elevated sulfate aerosol: Three-dimensional coupled model simulations, J. Geophys. Res., 106, 27,255-27,275, 2001.

Avery, M. A., D. J. Westberg, H. E. Fuelberg, R. E. Newell, B. E. Anderson, S. A. Vay, G. W. Sachse, and D. R. Blake, Chemical transport across the ITCZ in the central Pacific during an El Nino-Southern Oscillation cold phase event in March-April 1999, J. Geophys. Res., 106, 32,539-32,553, 2001.

Avissar, R., E. Eloranta, K. Gurer, and G. J. Tripoli, An evaluation of the large eddy simulation option of the Regional Atmospheric Modeling System in simulating the convective boundary layer: A Fife case study, J. Atmos. Sci., 55, 1109-1130, 1998.

Bey I., D. J. Jacob, R. M. Yantosca, J. A. Logan, B. D. Field, A. M. Fiore, Q. Li, H. Y. Liu, L. J. Mickley, M. G. Schultz, Global modeling of tropospheric chemistry with assimilated meteorology: Model description and evaluation, J. Geophys. Res., 106, 23,073-23,095, 2001a.

Bey, I., D. J. Jacob, J. A. Logan, and R. M. Yantosca, Asian chemical outflow to the Pacific in spring: Origins, pathways, and budgets, J. Geophys. Res., 106, 23,097-23,113, 2001b.

Bhartia, P.K., R. D. McPeters, C. L. Mateer, L.E. Flynn, and C. Wellemeyer, Algorithm for the estimation of vertical ozone profile from the backscattered ultraviolet (BUV) technique, J. Geophys. Res., 101, 18793-18806, 1996.

Bjerknes, J., Extratropical cyclones, *Compendium of Meteorology*, T.F. Malone, Ed., Amer. Meteor. Soc., 577-598, 1951.Carmichael, G.R., I. Uno, M. J. Phadnis, Y. Zhang, and Y. Sunwoo, Tropospheric ozone production and transport in the springtime in east Asia, J. Geophys., Res. 103, 10,649-10,671, 1998.

Browell, E. V., M. A. Fenn, C. F. Butler, W. B. Grant, V. G. Brackett, J. W. Hair, M. A. Avery, R. E. Newell, Y. Hu, H. E. Fuelberg, D. J. Jacob, B. E. Anderson, E. L. Atlas, D. R. Blake, W. H. Brune, J. E. Dibb, A. Fried, B. G. Heikes, G. W.

Sachse, S. T. Sandholm, H. B Singh, R. W. Talbot, S. A. Vay, and R. J. Weber, Large-Scale Ozone and Aerosol Distributions, Air Mass Characteristics, and Ozone Fluxes Over the Western Pacific Ocean in Late-Winter/Early-Spring, J. Geophys. Res., this issue.

Carmichael, G. R., Uno I., Phadnis M. J., Zhang Y. and Sunwoo, Y. (1998) Tropospheric ozone production and transport in the springtime in east Asia, J. Geophysical Research, 103, 10649-10671.

Carmichael, G. R., Y. Tang, G. Kurata, I. Uno, D. G. Streets, J.-H. Woo, H. Huang, J. Yienger, B. Lefer, R. E. Shetter, D. R. Blake, A. Fried, E. Apel, F. Eisele, C. Cantrell, M. A. Avery, J. D. Barrick, G. W. Sachse, W. L. Brune, S. T. Sandholm, Y. Kondo, H. B. Singh, R. W. Talbot, A. Bandy, A. D. Clarke, and B. G. Heikes, Regional-Scale Chemical Transport Modeling in Support of Intensive Field Experiments: Overview and Analysis of TRACE-P Observations, J. Geophys. Res., this issue.

Carpenter, M. H. A High-Order Compact Numerical Algorithm for Supersonic Flow, *Twelfth International Conference on Numerical Methods in Fluid Dynamics*, K. W. Morton, ed., Vol 371 of *Lecture Notes in Physics*, Springer-Verlag, pp254-258, 1990.

Chen, S. J., Y.-H. Kuo, P.-Z. Zhang, and Q.-F. Bai, Synoptic Climatology of Cyclogenesis over East Asia, 1958-1987, Mon. Wea. Rev., 119, 1407-1418, 1991.

Colella, P. and P. R. Woodward, The Piecewise Parabolic Method (PPM) for gas-dynamical simulations, J. Comp. Phys., 54 (1984), pp. 174-201.

Crawford, J., D. Davis, G. Chen, J. Bradshaw, S. Sandholm, Y. Kondo, S. Liu, E. Browell, G. Gregory, B. Anderson, G. Sachse, J. Collins, J. Barrick, D. Blake, R. Talbot, and H. Singh, An assessment of ozone photochemistry in the extratropical western North Pacific: Impact of continental outflow during the late winter/early spring, J. Geophys. Res., 102, 28,469-28,487, 1997.

Crawford, J., D. Davis, J. Olson, G. Chen, S. Liu, G. Gregory, J. Barrick, G. Sachse, S. Sandholm, B. Heikes, H. Singh, and D. Blake, Assessment of upper tropospheric HOx sources over the tropical Pacific based on NASA GTE/PEM data: Net effect

on Hox and other photochemical parameters, J. Geophys. Res., 104, 16,255-16,273, 1999.

Danielsen, E. F., R. S. Hipskind, S. E. Gaines, G. W. Sachse, G. L. Gregory, and G. F. Hill, Three-dimensional analysis of potential vorticity associated with tropopause folds and observed variations of ozone and carbon monoxide, *J. Geophys. Res*, **92**, 2103-2111, 1987.

DeMore, W. B., S. P. Sander, D. M. Goldan, R. F. Hampson, M. J. Kurylo, C. J. Howard, A. R. Ravishankara, C. E. Kolb and M. J. Molina, 1997: Chemical kinetics and photochemical data for use in stratospheric modeling. Evaluation No. 12, JPL Publication 97-4, Jet Propulsion Laboratory, California Institute of Technology, Pasadena, CA.

Duncan et al., "Interannual and Seasonal Variability of Biomass Burning Emissions Constrained by Satellite Observations", submitted to J. Geophys. Res., 2002.

Eckman, R. S., W. L. Grose, R. E. Turner, W. T. Blackshear, and J. M. Russell III, Stratospheric trace constituents simulated by a three-dimensional general circulation model: Comparison with UARS data, J. Geophys. Res., 100, 13,951-13,966, 1995.

Emmons, L. K., D. A. Hauglustaine, J.-F. Muller, M. A. Carroll, G. P. Brasseur, D. Brunner, J. Staehelin, V. Thouret, A. Marenco, Data composites of airborne observations of tropospheric ozone and its precursors J. Geophys. Res. 105 , 20,497-20,538, 2000.

Fishman, J. and A. E. Balok, Calculation of daily tropospheric ozone residuals using TOMS and empirically improved SBUV measurements: Application to an ozone pollution episode over the eastern United States, J. Geophys. Res., 104, 30,319-30,340, 1999.

Fishman, J., A. E. Balok, and F. M. Vukovich, Observing tropospheric trace gases from space: Recent advances and future Capabilities, *Adv. Space Res.* **29,** 1625-1630, 2002.

Fishman, J., A. E. Wozniak, and J. K. Creilson, Global distribution of tropospheric ozone from satellite measurements using the empirically corrected tropospheric ozone

residual technique: Identification of the regional aspects of air pollution, *Atmos. Chem. Phys. Discuss..,* **3**, 1-24, 2003 (www.atmos-chem-phys.org/acpd/3/1)

Fishman, J., C. E. Watson, J. C. Larsen, and J. A. Logan, Distribution of Tropospheric Ozone Determined from Satellite Data., J. Geophys. Res, 95, 3599-3617, 1990.

Fishman, J., Ozone in the troposphere; in Ozone in the Free Atmosphere (Chapter 4), R. C. Whitten and S. S. Prasad, editors; VonNostrand, Reinhold Publ. Co., New York,161-195, 1985.

Fishman, J., and P. J. Crutzen, The origin of ozone in the troposphere, *Nature*, **274**, 855-858, 1978.

Folkins, I., and C. Appenzeller, Ozone and potential vorticity at the subtropical tropopause break, J. Geophys. Res., 101, 18,787-18,792, 1996.

Fuelberg, H. E., C. M. Kiley, J. R. Hannan, D. J. Westberg, M. A. Avery, R. E. Newell, Atmspheric transport during the TRAnsport and Chemical Evolution over the Pacific (TRACE-P) experiment, J. Geophys. Res., this issue.

Galbally , I. E. and C. R. Roy, Destruction of ozone at the earths' surface, Q.J.R. Meteorol. Soc., 106, 599-620, 1980.

Hitchman, M. H., M. L. Buker, and G. J. Tripoli, Influence of synoptic waves on column ozone during Arctic summer 1997. J. Geophys. Res., 104, 26,547- 26,564, 1999.

Hitchman, M. H., M. L. Buker, G. J. Tripoli, E. V. Browell, W. B. Grant, T. J. McGee, and J. F. Burris, Non-orographic generation of arctic PSCs during December 1999, J. Geophys. Res., 108, 1029, 2003.

Hoell, J.M., et al., The Pacific Exploratory Mission-West Phase B: February-March 1994. J. Geophys. Res., 102, 28,223-28,240, 1997.

Hoerling, M. P., T. K., Schaack, and A. J. Lenzen, A global analysis of stratospheric-tropospheric exchange during northern winter, Mon. Weather Rev., 121, 162-172, 1993.

Holton, J. R., P. H. Haynes, M. E. McIntyre, A. R. Douglas, R. B. Rood, L. Pfister, Stratosphere-Troposphere Exchange, Reviews of Geophysics, 33, 403-439, 1995.

Holtslag, A. A. M. and B. Boville, Local versus nonlocal boundary-layer diffusion in a global climate model. J. Climate, **6**, 1825-1842, 1993.

Huesmann, A. S. and M. H. Hitchman, The 1978 shift in the NCEP reanalysis stratospheric quasibiennial oscillation, Geophys. Res., Letts., January 2003.

Jacob, D. J., J. H. Crawford, M. M. Kleb, V. E. Conners, R. J. Bendura, L. Raper, The TRAnsport and Chemical Evolution over the Pacific (TRACE-P) Experiment, J. Geophys. Res., this issue.

Jaffe, D., T. Anderson, D. Covert, R. Kotchenruther, B. Trost, J. Danielson, W. Simpson, T. Bernsten, S. Karlsdottir, D. Blake, J. Harris, G. Carmichael, and I. Uno, Transport of Asian air pollution to North America, *Geophys. Res. Lett*., 26, 711-714, 1999.

Johnson, D. R., T. H. Zapotocny, F. M. Reames, B. J. Wolf and R. B. Pierce, 1993: A comparison of simulated precipitation by hybrid isentropic-sigma and sigma models. *Mon. Wea. Rev*., **121**, 2088-2114.

Johnson, D. R., A. J. Lenzen, T. H. Zapotocny, and T. K. Schaack, 2000: Numerical uncertainties in the simulation of reversible atmospheric processes and entropy conservation. *J. Climate*, **13**, 3860-3884.

Johnson, D. R., A. J. Lenzen, T. H. Zapotocny and T. K. Schaack, 2002: Entropy, numerical uncertainties and modeling of atmospheric hydrologic processes: Part B. *J. Climate*, **15**, 1777-1804.

Kaneyasu, N., K. Takeuchi, M. Hayashi, S.-I. Fujita, I. Uno, and H. Sasaki, Outflow patterns of pollutants from east Asia to the north Pacific in the winter monsoon, *J. Geophys. Res*., 105, 17361-17377, 2000.

Kiehl, J. T., J. J. Hack, G. B. Bonan, B. A. Boville, B. P. Briegleb, D. L. Williamson and P. J. Rasch (1996): Description of the NCAR Community Climate Model (CCM3). NCAR/TN-420+STR.

Kiehl, J. T., J. J. Hack, G. B. Bonan, B. B. Boville, D. L. Williamson and P. J. Rasch, The National Center for Atmospheric Research Community Climate Model: CCM3. J. Climate, 11, 1998.

Kiley, C. M., H. E. Fuelberg, P. I. Palmer, D. J. Allen, G. R. Carmichael, D. J. Jacob, C. Mari, R. B. Pierce, K. E. Pickering, Y. Tang, O. Wild, T. D. Fairlie, J. A. Logan, G. W. Sachse, D. G. Streets, An intercomparison and evaluation of aircraft-

derived and simulated CO from seven chemical transport models during the TRACE-P experiment, J. Geophys. Res., this issue.

Koike, M., Y. Kondo, K. Kita, N. Takegawa, Y. Masue, Y.Miyazaki, M. W. Ko, R. Weber, D. C. Thornoton, G. Sachse, S. Vay, D. Blake, D. Streets, F. Flocke, F. Eisele, S. Sandholm, H. B. Singh, and R. W. Talbot, Export of anthropogenic reactive nitrogen and sulfur compounds from the East Asia region in spring, J. Geophys. Res., this issue.

Lamaque, J.-F. and P. G. Hess, Cross-Tropopause Mass Exchange and Potential Vorticity Budget in a Simulated Tropopause Folding, J. Atmos. Sci., 51, 2246-2269, 1994.

Lelieveld, J., and Dentener, F. J., What controls tropospheric ozone? J. Geophys. Res., 105, 3531-3551, 2000.

Levy, H., II, J. D. Mahlman, W. J. Moxim, and S. C. Liu, Tropospheric ozone: The role of transport. J. Geophys. Res., 90(D2), 3753-3772, 1985.

Liu, H., D. J. Jacob, L. Y. Chan, S. J. Oltmans, I. Bey, R. M. Yantosca, J. M. Harris, B. N. Duncan, R. V. Martin, Sources of tropospheric ozone along the Asian Pacific Rim: An Analysis of ozoneonde observations, accepted to J. Geophys. Res, 2002.

Logan, J. A., An analysis of ozoneonde data for the troposphere: Recommendations for testing 3-D models, and development of a gridded climatology for tropospheric ozone*, J. Geophys. Res*., **104**, 16,115-16,149, 1999.

Mecikalski, J. R., and G. J. Tripoli, Inertial available kinetic energy a nd the dynamics of tropical plume formation, Mon. Weather Rev., 126, 2200- 2216, 1997.

Muller, J. F. and G. Brasseur, IMAGES: A three-dimensional chemical transport model of the global troposphere, J. Geophys. Res., 100, 16,445-16,490, 1995.

Palmen, E. and C. W. Newton, *Atmospheric Circulation Systems Their Structure and Physical Interpretation*, International Geophysics Series, Volume 13, Academic Press, 1969.

Pierce, R. B., J-U Grooss, W. L. Grose, J. M. Russell III, P. J. Crutzen, T. D. Fairlie, G. Lingenfelser: Photochemical Calculations Along Airmass Trajectories During ASHOE/MAESA, J. Geophy. Res., 102, 13,153-13,167, 1997.

Pierce, R. B., J. A. Al-Saadi, T. D. Fairlie, J. R. Olson, R. S. Eckman, W. L. Grose, G. S. Lingenfelser, J. M. Russell III, "Large-scale stratospheric ozone photochemistry

and transport during the POLARIS campaign," J. Geophys. Res., 104, 26525-26545, 1999.

Pierce, R. B., J.A. Al-Saadi, R. S. Eckman, T. D. Fairlie, W. L. Grose, M. M. Kleb,M. Natarajan, J. R. Olson, Dynamical climatology of the NASA Langley Research Center Interactive Modeling Project for Atmospheric Chemistry and Transport (IMPACT) Model, J. Geophys. Res., 105, 29,109-29,134, 2000.

Pierce, R. B., et al., Large-scale chemical evolution of the Arctic vortex during the 1999-2000 winter: HALOE/POAM3 Lagrangian photochemical modeling for the SAGE III Ozone loss and validation experiment (SOLVE) campaign, J. Geophys. Res., 107, 8317, doi:10.1029/2001JD001063, 2002 [printed 108(D5), 2003]

Pokrandt, P. J., G. J. Tripoli, and D. D. Houghton, Processes leading to the formation of mesoscale waves in the midwest cyclone of 15 December 1987, Mon. Weather Rev., 124, 2726-2752, 1996.

Postel, G. A., and M. H. Hitchman, Climatology of Rossby Wave Breaking Along the Subtropical Tropopause. *J. Atmos. Sci.*, **56**, 359-373, 1999

Price, C., J. Penner, and M. Prather. NO_x from lightning: 2. Constraints from the global atmospheric electric circuit. J. Geophys. Res*., 102*, 5942-5951, 1997.

Sander, S. P., R. R. Friedl, W. B. DeMore, A. R. Ravishankara, D. M. Golden, C. E. Kolb, M. J. Kurylo, R. F. Hampson, R. E. Huie, M. J. Molina and G. K. Moortgat, 2000: Chemical Kinetics and Photochemical Data for Use in Stratospheric Modeling. Supplement to Evaluation No. 12 - Update of Key Reactions and Evaluation No.13, JPL Publication 00-3, Jet Propulsion Laboratory, California Institute of Technology, Pasadena, CA.

Seo, K. H. and K. P. Bowman, A climatology of isentropic cross-tropopause exchange, J. Geophys. Res., 106, 28,159-28,172, 2001.

Stolarski, R. S., S. L. Baughcum, W. H. Brune, A. R. Douglas, D. W. Fahey, R. F. Friedl, S. C. Liu, R. A. Plumb, L. R. Poole, H.L. Wesoky, and D. R. Worsnop, 1995 Scientific Assesment of the Atmospheric Effects of Stratospheric Aircraft, NASA Reference Publication 1281, National Aeronautics and Space Administration, Washington, DC, 1995.

Streets, D. G., T. C. Bond, G. R. Carmichael, S. D. Frenandes, Q. Fu, D. He, Z. Klimont, S. M. Nelson, N. Y. Tsai, M. Q. Wang, J.-H., Woo, and K. F. Yarber, An inventory of gaseous and primary aerosol emissions in Asia in the year 2000, J. Geophys. Res., this issue.

Tripoli, G. J., A nonhydrostatic numerical model designed to simulate scale interaction. Mon. Wea. Rev., 120, 1342-1359, 1992.

Wang, Y., D. J. Jacob, and J. A. Logan, Global simulation of tropospheric O_3-NO_x-hydrocarbon chemistry, 3. Origin of tropospheric ozone and effects of nonmethane hydrocarbons, *J. Geophys. Res*, **103**,10,757-10,767, 1998.

Wei, M-Y, 1987, "A new formulation of the exchange of mass and trace constituents between the stratosphere and troposphere," J. Atmos. Sci., 44, No.20, 3079-3086.

Dentener F. J. and P. J. Crutzen, Reaction of N2O5 on tropospheric aerosols: impact on the global distributions of NOx, O_3 and OH, J. Geophys.Res., 98, 7149-7163, 1993

Wirth, V., and J. Egger, Diagnosing extratropical synoptic-scale stratosphere-troposphere exchange: a case study, Q. J. R. Meteorol. Soc., 125, 635-655, 1999.

WMO World Data Center for Greenhouse Gases (WDCGG) DATA Catalog No. 4, 148pp, December, 1993.

Yienger, J. J. and H. Levy. Empirical model of global soil-biogenic NO_x emissions. J. Geophys. Res*., 100*, 11447-11464, 1995.

Zapotocny, T. H., D. R. Johnson, and F. M. Reames, Development and initial test of the University of Wisconsin global isentropic-sigma model. Mon. Wea. Rev., 122, 2160-2178, 1994.

Zapotocny, T. H., A. J. Lenzen, D. R. Johnson, F. M. Reames, P. A. Politowicz, and T. K. Schaack, 1996: Joint distributions of potential vorticity and inert trace constituent in CCM2 and UW θ–σ model simulations. *Geophys. Res. Let.*, **23**, 2525-2528.

Zapotocny, T. H., A. J. Lenzen, D. R. Johnson, F. M. Reames, and T. K. Schaack, 1997a: A comparison of inert trace constituent transport between the University of Wisconsin isentropic-sigma model and the NCAR Community Climate Model. *Mon. Wea. Rev*., **125**, 120-142.

Zapotocny, T. H., D. R. Johnson, T. K. Schaack, A. J. Lenzen, F. M. Reames, P. A. Politowicz, and Z. Yuan, 1997b: Simulations of tropospheric joint distributions in the UW θ–σ model and CCM2. *Geophys. Res. Lett.,* **24**, 865-868.

Zhang, G. J. and N. A. McFarlane, Sensitivity of climate simulations to the parameterization of cumulus convection in the CCC-GCM. *Atmos.-Ocean*, **3**, 407-446, 1995.

Figure Captions:

Figure 1. Climatological February-April tropospheric ozone residual (TOR) in D.U. (colored), East Asian DC8 (red) and P3B (black) flights during TRACE-P, March 2001 200mb winds (m/s) (dashed contours) and geopotential heights (dam) (solid contours).

Figure 2. Schematic illustration of the discrete flux calculation.

Figure 3. The upper and lower left panels show March mean column ozone distributions (colored) from TOMS (upper) and the $RAQMS_G$ prediction (lower). Thick black lines indicate the boundaries of the $RAQMS_R$ domain. The mean pressure of the thermal tropopause, obtained from the UW $\theta-\eta$ model predictions, is contoured in white. The middle panels show March 2001 monthly mean tropospheric ozone residuals (TOR) the $RAQMS_G$ tropospheric column ozone prediction. The right hand panels show comparisons between composite East Asian tropospheric ozone distributions obtained by the UV DIAL instrument and from the $RAQMS_N$ predictions during TRACE-P. The 20, 40, 60, 80, 100, and 200ppbv ozone mixing ratios are contoured. The mean altitude of the thermal tropopause determined from the UW-NMS prediction is indicated in black.

Figure 4. The upper panel shows March 2001 zonal mean comparisons between TOMS and $RAQMS_G$ total column ozone. The middle panel shows March 1-25th zonal mean comparisons between TOMS/SBUV and $RAQMS_G$ TOR. The lower panel shows March 2001 East Asian tropospheric column ozone from TOMS/SBUV, $RAQMS_G$, and $RAQMS_N$ averaged between 120^o-150^{o}E and DIAL and DIAL-sampled $RAQMS_R$ composites for flights between March 9-31, 2001.

Figure 5. The upper left panel shows TOMS column ozone for March 17, 2001 within the TRACE-P domain. The thick black and red line indicates the flight track for DC8 flight 11. The $RAQMS_G$ 06Z tropopause pressure is shown in white contours. The upper right panel shows the time series of DIAL ozone measurements for DC8 Flight 11. The lower left panel shows a north-south cross-section of ozone mixing ratio averaged between 131^o-138^{o}E at 06Z from the $RAQMS_N$ prediction (this longitude band is

indicated by the two black lines extending N-S in the upper left panel). The flight track is indicated in thick black lines (with the section of the flight within this cross-section indicted by thick red), dashed lines indicate isentropes, and the zonal wind within the subtropical jet is contoured. The lower right panel shows a comparison between the $RAQMS_N$ prediction (dashed) and in situ (solid) ozone for DC8 Flight 11. The altitude of the aircraft is indicated by a dotted line.

Figure 6. Altitude binned results of statistical analysis of $RAQMS_N$ and in situ measurements. Within each altitude bin, the distributions are characterized by their median, 50 percentile, and 90 percentiles (vertical line, box, and horizontal lines, respectively). The upper left panel shows results for O_3. Results for NO_x are shown in the upper right panel. Diurnally averaged gross photochemical formation and destruction of ozone are shown in the lower panels.

Figure 7. Zonal averaged flux of O_3 across the tropopause within the $RAQMS_N$ model domain for the period from March 07 –April 12, 2001. The components of the O_3 flux and zonal averaged tropopause altitude are also shown.

Figure 8. Time averaged zonal mean O_3 number density within the $RAQMS_N$ domain (upper left), horizontal O_3 fluxes of on western (upper middle), eastern (upper right), southern (lower middle) and northern (lower right) boundaries, and 6hr averaged net O_3 production (lower left) from March 07^{th} to April 12^{th}, 2001.

Figure 9. Time series of spatially integrated O_3 budget terms within the $RAQMS_N$ domain. The sum of the horizontal fluxes is shown in the upper left panel. The upper right panel shows the time series of O_3 fluxes through the tropopause. The lower left panel shows the time series of net O_3 production (solid) and deposition (dotted). The lower right panel shows a time series of the accumulated (instantaneous-initial) O_3 within the $RAQMS_N$ domain (thick solid) along with the ozone accumulation predicted from the sum of the individual net tendencies in our budget calculation (thick dotted). The predicted ozone accumulation when horizontal fluxes (dash-dot-dot-dot) STE (dashed),

or net production (dash-dot) are excluded is also shown to assess the relative importance of these terms in the overall budget.

Table 1: Chemical Constituents Used in RAQMS

O_3
O
NO
NO_2
HNO_3
HNO_2
NO_3
H_2O_2
OH
HO_2
N_2O
N_2O_5
H_2O
HCl
CF_2Cl_2
$CFCl_3$
$ClONO_2$
CH_4
CH_2O
CO
CH_3OOH
CCl_4
CH_3Cl
Cl
ClO
H
O(1D)
N
Cl_2
CH_3
HCO
CH_3O_2
CH_3O
ClO_2
O_2
H_2
CH_3CCl_3
HOCl
HO_2NO_2
Cl_2O_2
OclO
Br
BrCl
BrO
HBr
HOBr
$BrONO_2$
CH_3Br
CF_3Br
CF_2ClBr
HF
CFClO
CF_2O

Table 2: Transported Chemical Families and Species

Ox
NOy
HNO_3
Cl_y
N_2O_5
H_2O_2
HCl
$ClONO_2$
OclO
N_2O
CFC13 (F11)
CF_2Cl_2 (F12)
CCl_4
CH_3Cl
CH_3CCl_3 (MTCFM)
Br_y
CH_3Br
CF_3Br (H1301)
CF_2ClBr (H1211)
HF
CFClO
CF_2O
CH_4
HOCl
HO_2NO_2
H_2O (from Met Model)
NO_3
NO_2
CH_2O
CH_3OOH
CO
HBr
$BrONO_2$
HOBr
BrCl
Cl_2

Table 3: Average Ozone Budget within $RAQMS_N$ domain during TRACE-P

Average Tropopause Flux (STE)	0.217 Tg/day
Average Gross Formation (F)	1.469 Tg/day
Average Gross Destruction (D)	-1.097 Tg/day
Average Surface Deposition (Dep)	-0.546 Tg/day
Sum of Average STE+F+D+Dep	**0.043 Tg/day**
Average Western Boundary Flux	3.493 Tg/day
Average Eastern Boundary Flux	-5.253 Tg/day
Average Southern Boundary Flux	0.073 Tg/day
Average Northern Boundary Flux	1.656 Tg/day
Sum of Average Boundary Fluxes	**-0.030 Tg/day**
Average Computed Accumulated O3	1.041 Tg
Average Actual Accumulated O3	0.966 Tg

(+)=Regional Increase, (-)=Regional Decrease, Averages from March 07 –April 12, 2001

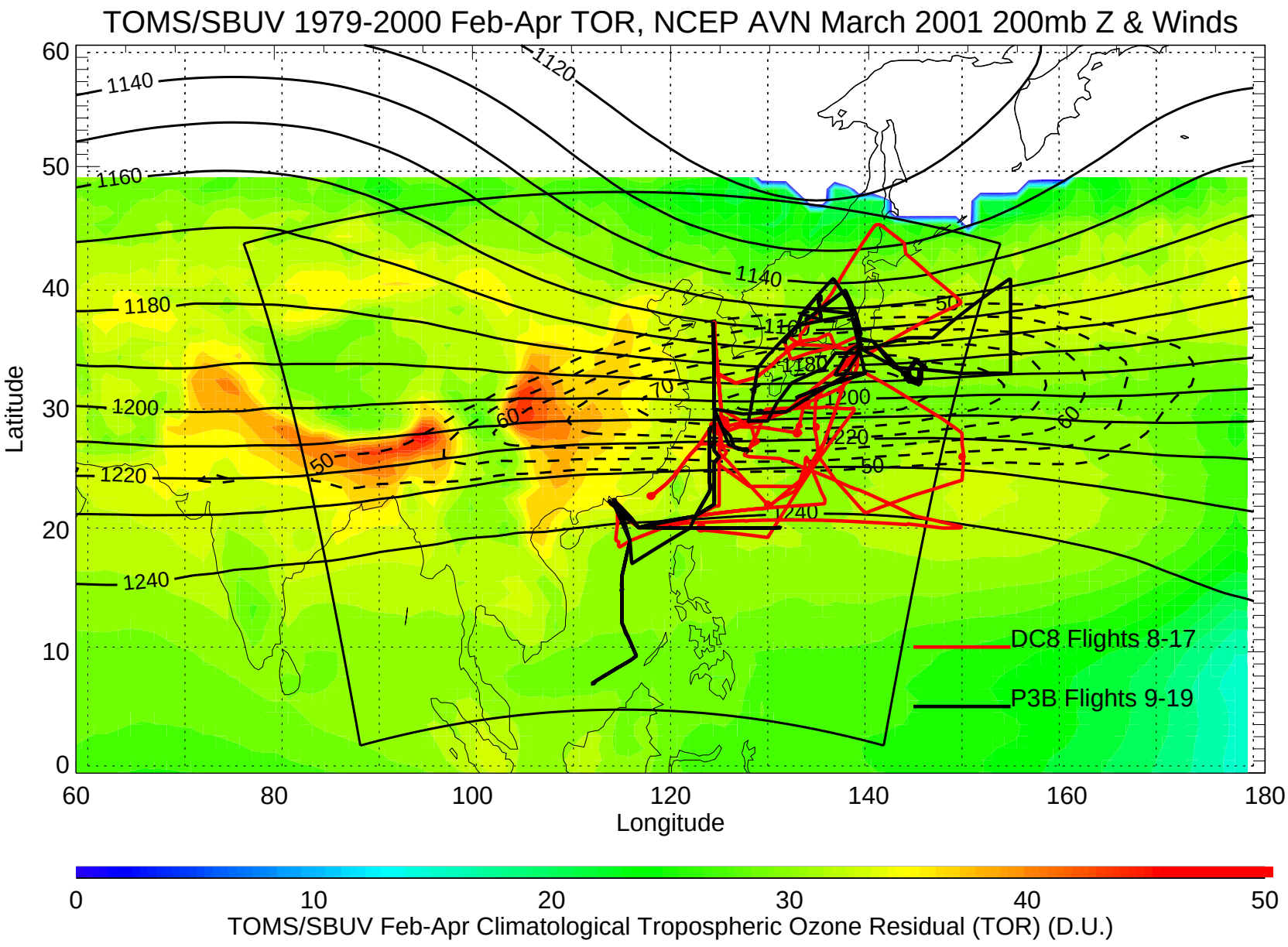
TOMS/SBUV 1979-2000 Feb-Apr TOR, NCEP AVN March 2001 200mb Z & Winds
Latitude
Longitude
60
50
40
30
20
10
0
60
80
100
120
140
160
180
1120
1140
1160
1180
1200
1220
1240
50
60
70
DC8 Flights 8-17
P3B Flights 9-19
0
10
20
30
40
50
TOMS/SBUV Feb-Apr Climatological Tropospheric Ozone Residual (TOR) (D.U.)

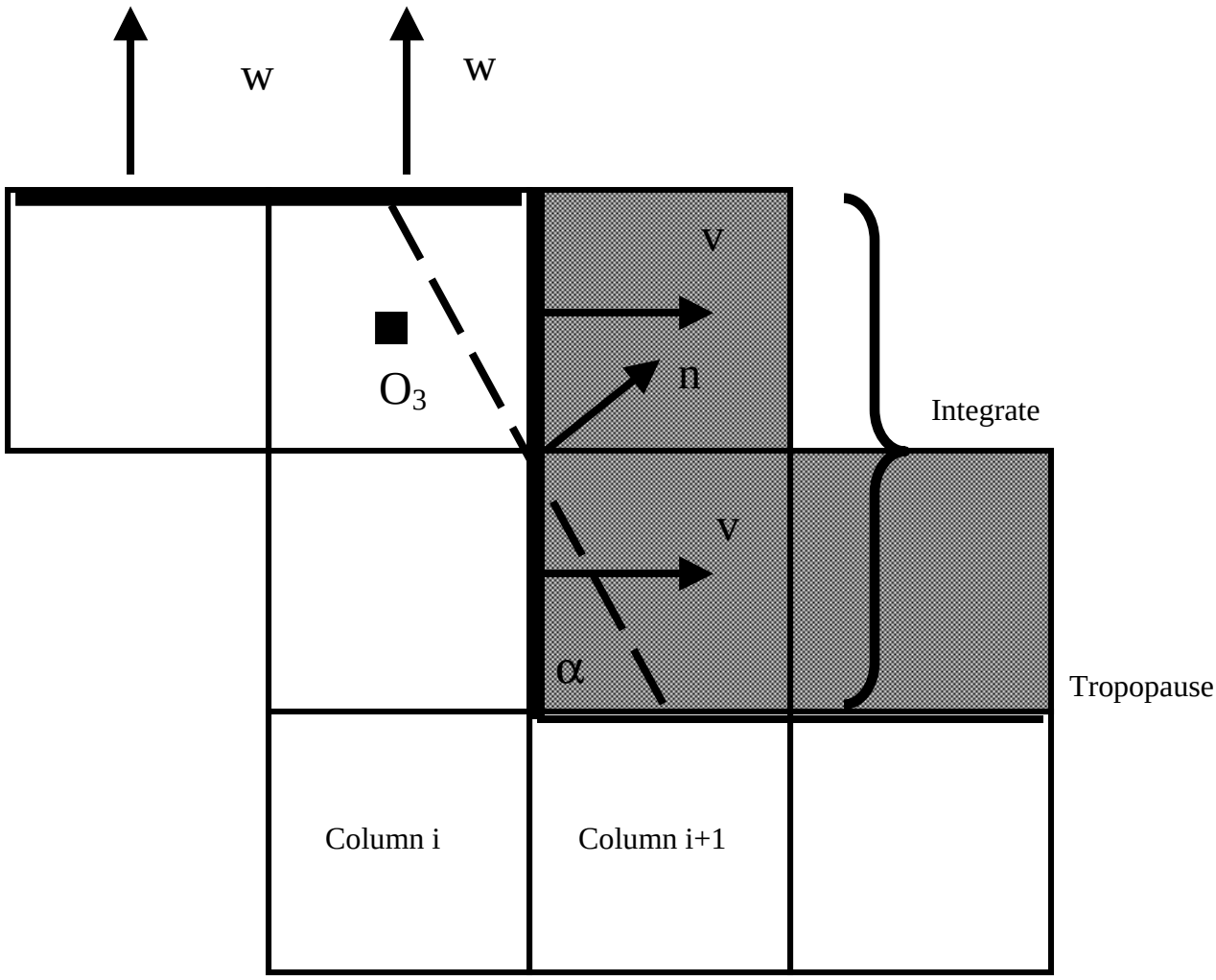
w
w
v
n
O_3
Integrate
v
α
Tropopause
Column i
Column i+1

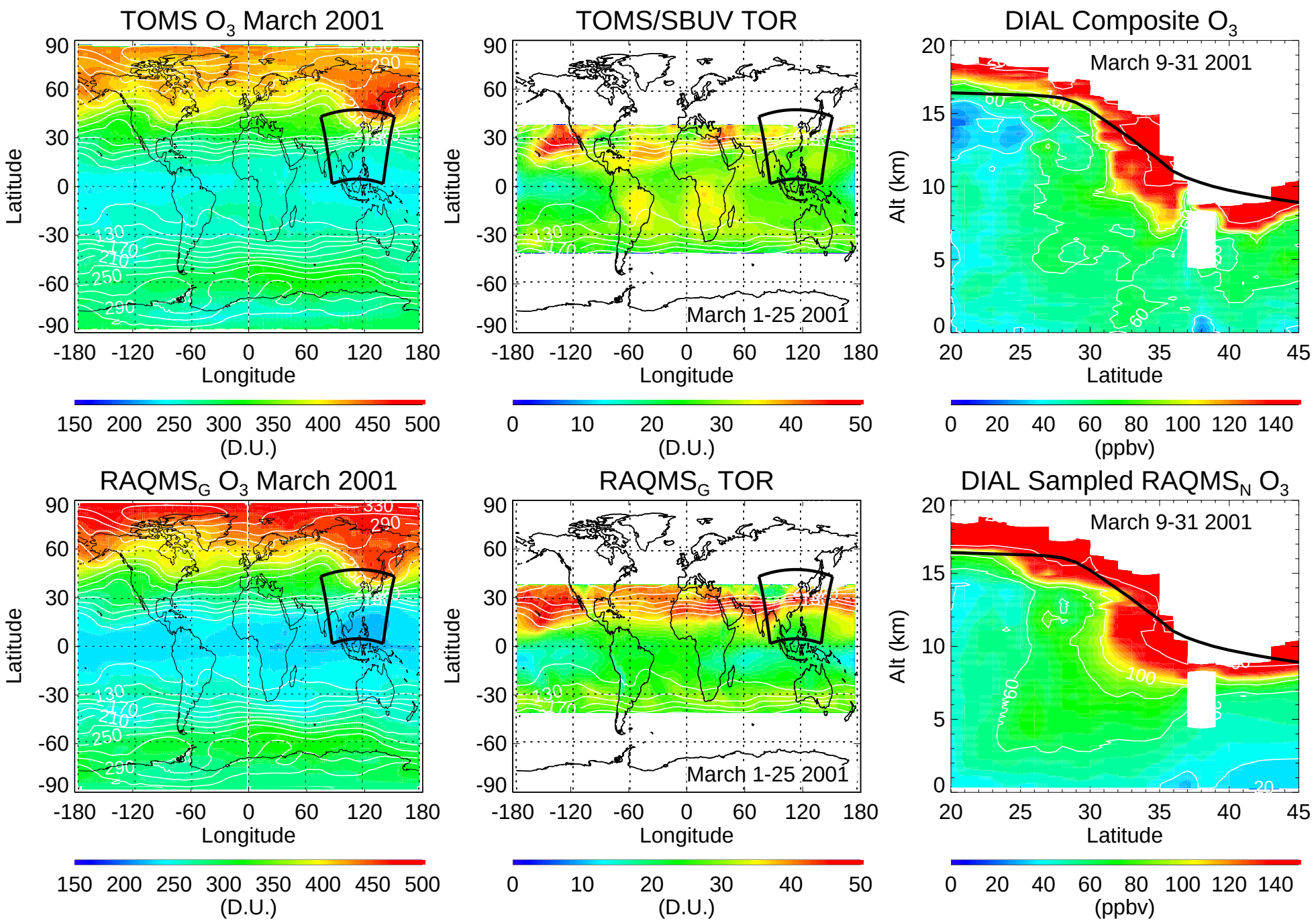
TOMS O_3 March 2001
Latitude
Longitude
90
60
30
0
-30
-60
-90
-180 -120 -60 0 60 120 180
290
250
210
170
130
150 200 250 300 350 400 450 500
(D.U.)
TOMS/SBUV TOR
March 1-25 2001
0 10 20 30 40 50
(D.U.)
DIAL Composite O_3
March 9-31 2001
Alt (km)
20
15
10
5
0
20 25 30 35 40 45
Latitude
0 20 40 60 80 100 120 140
(ppbv)
$RAQMS_G$ O_3 March 2001
$RAQMS_G$ TOR
DIAL Sampled $RAQMS_N$ O_3

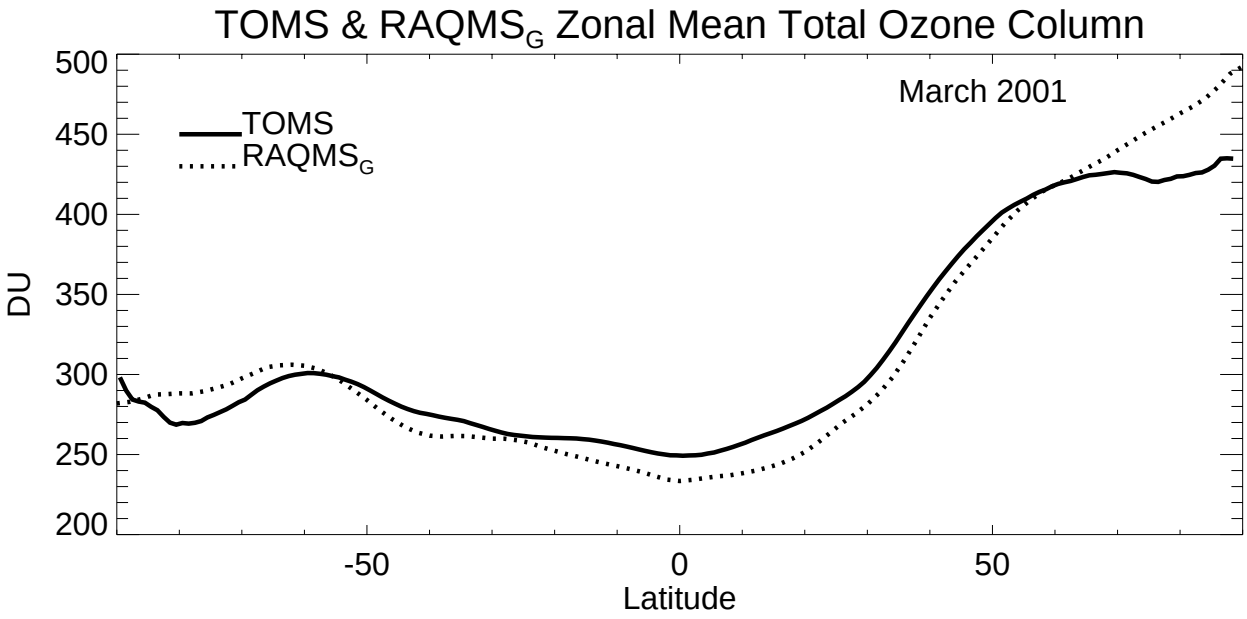
TOMS & RAQMS$_G$ Zonal Mean Total Ozone Column
March 2001
TOMS
RAQMS$_G$
DU
Latitude

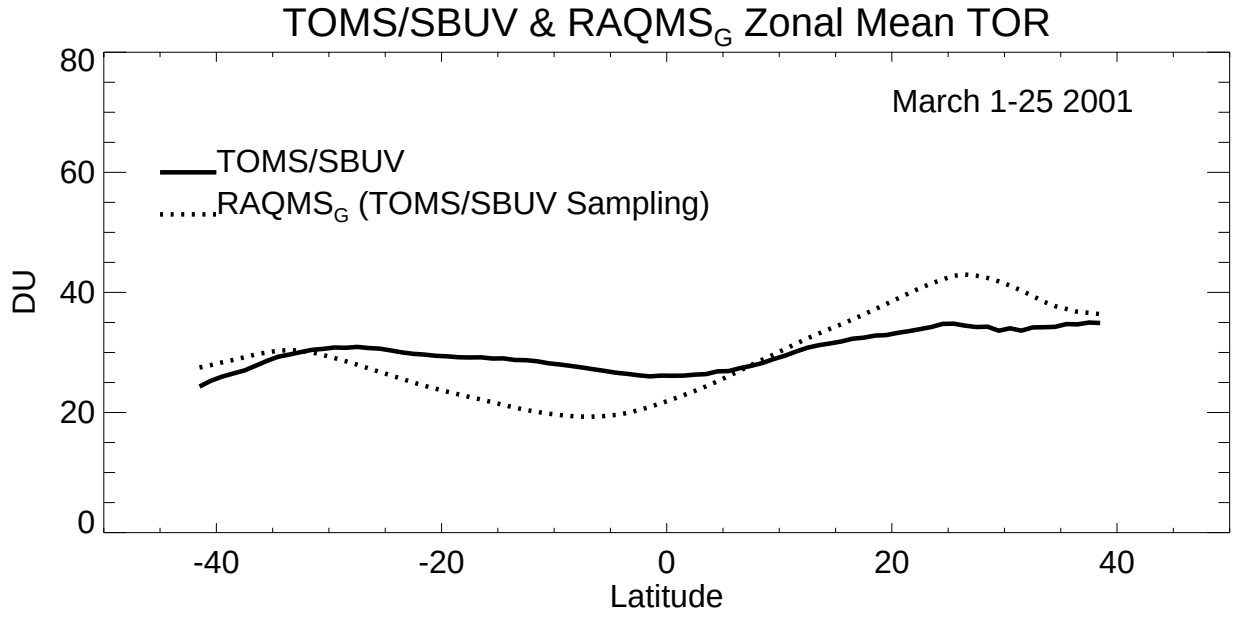
TOMS/SBUV & RAQMS$_G$ Zonal Mean TOR
March 1-25 2001
TOMS/SBUV
RAQMS$_G$ (TOMS/SBUV Sampling)
DU
Latitude

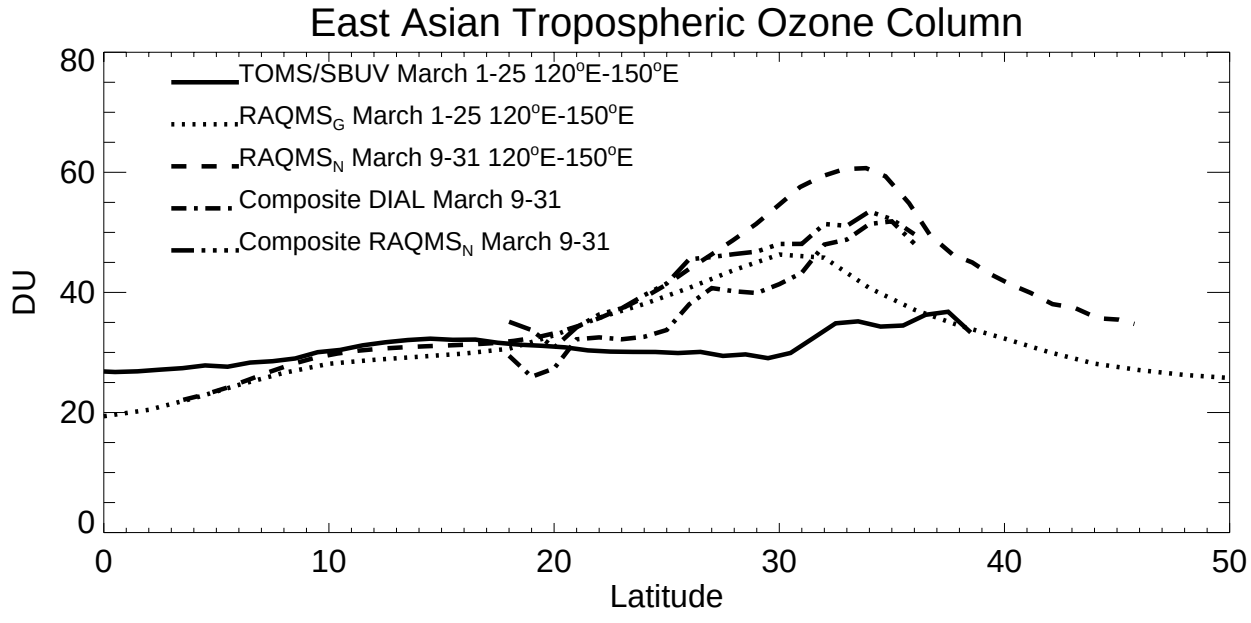
East Asian Tropospheric Ozone Column
TOMS/SBUV March 1-25 120°E-150°E
RAQMS$_G$ March 1-25 120°E-150°E
RAQMS$_N$ March 9-31 120°E-150°E
Composite DIAL March 9-31
Composite RAQMS$_N$ March 9-31
DU
Latitude

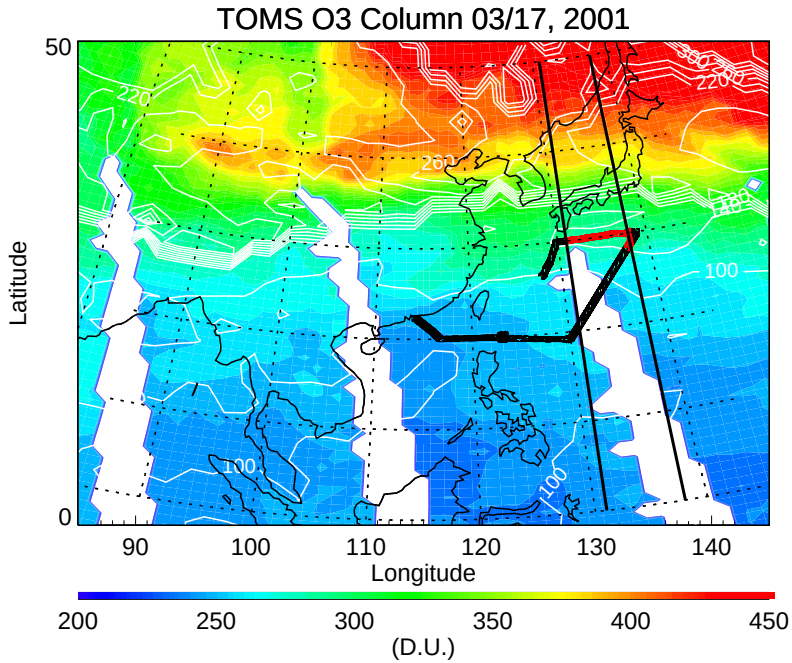
TOMS O3 Column 03/17, 2001
Latitude
Longitude
(D.U.)

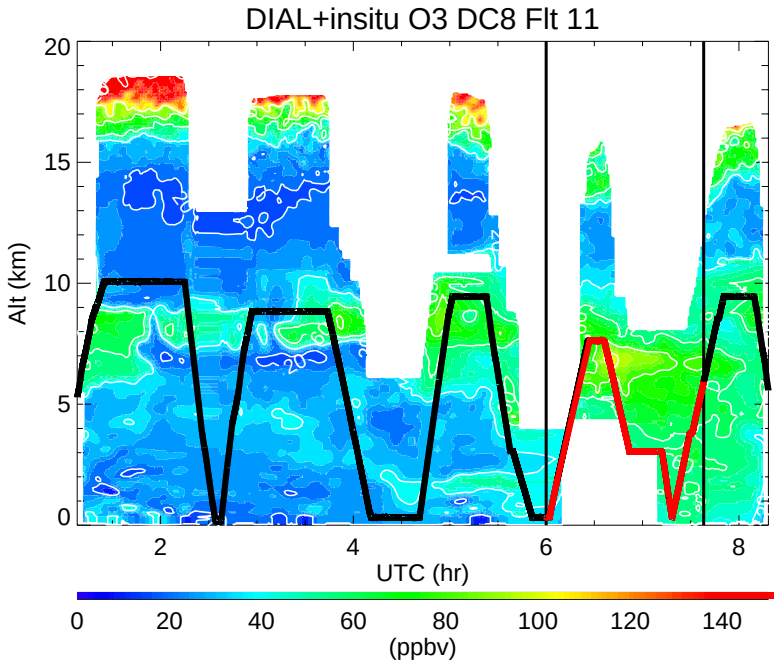
DIAL+insitu O3 DC8 Flt 11
Alt (km)
UTC (hr)
(ppbv)

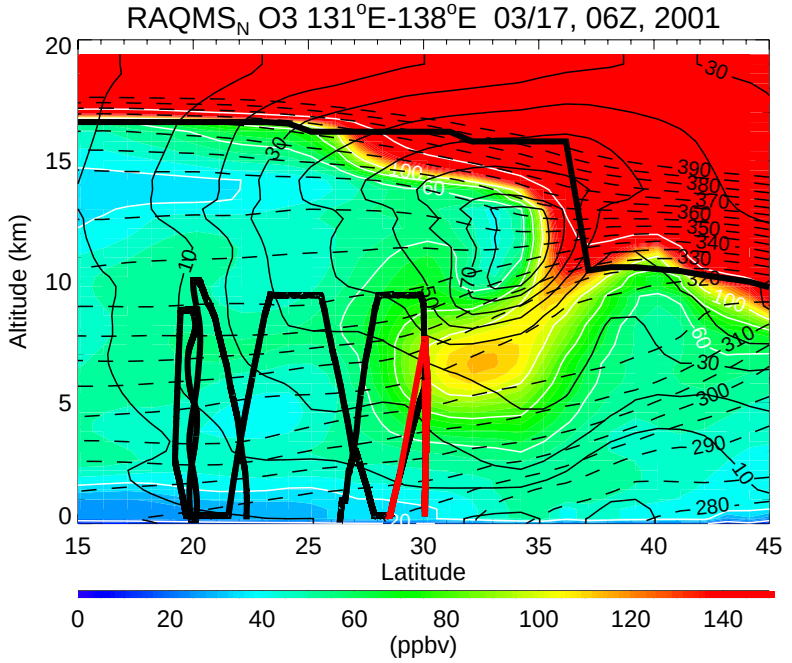
RAQMS$_N$ O3 131°E-138°E 03/17, 06Z, 2001
Altitude (km)
Latitude
(ppbv)

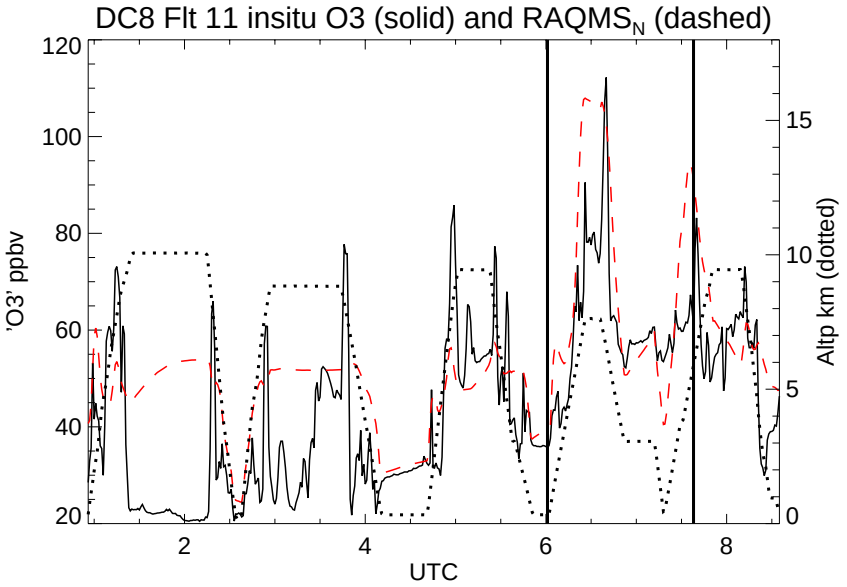
DC8 Flt 11 insitu O3 (solid) and RAQMS$_N$ (dashed)
'O3' ppbv
Altp km (dotted)
UTC

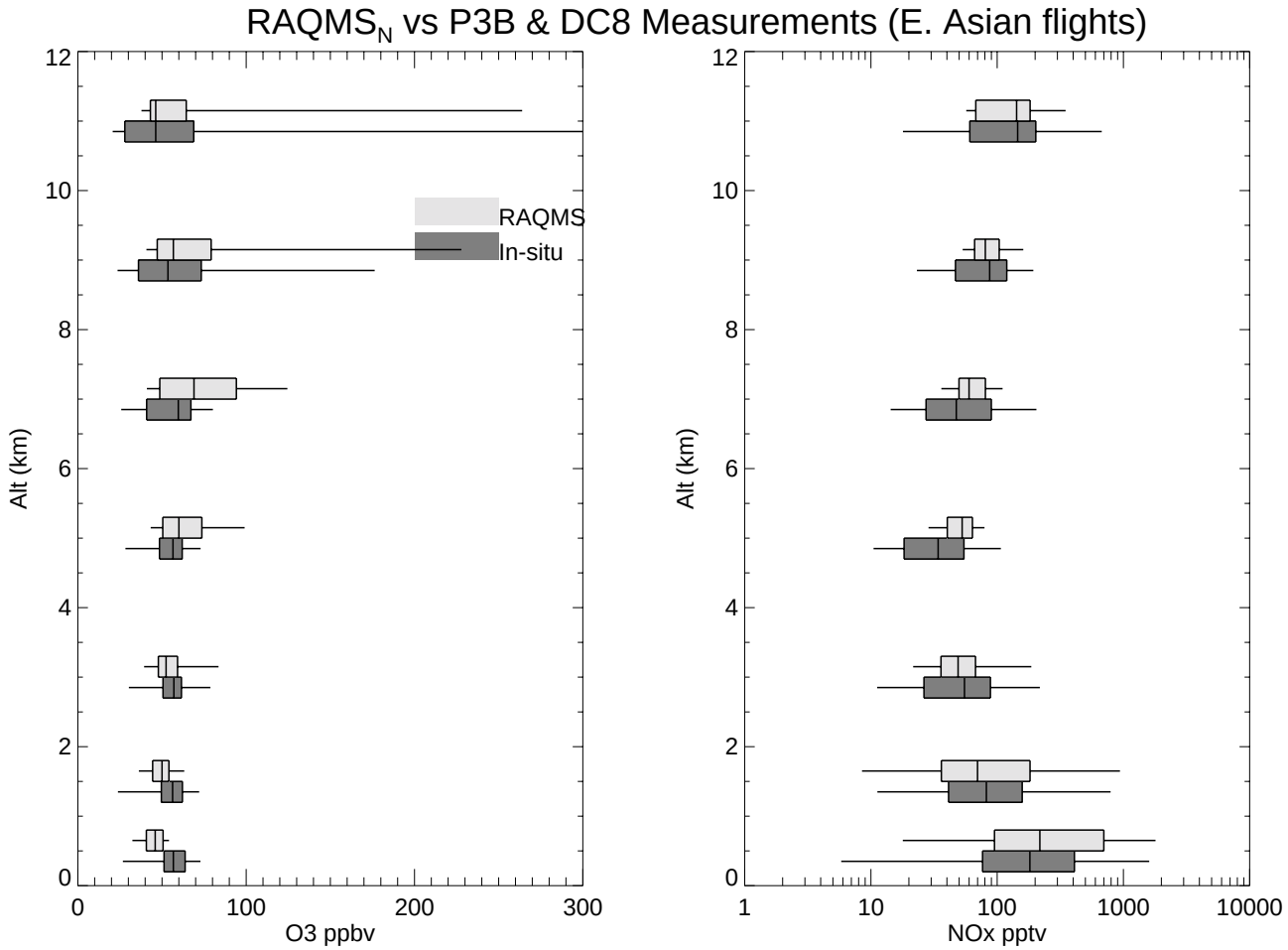
RAQMS$_N$ vs P3B & DC8 Measurements (E. Asian flights)
RAQMS
In-situ
Alt (km)
O3 ppbv
NOx pptv

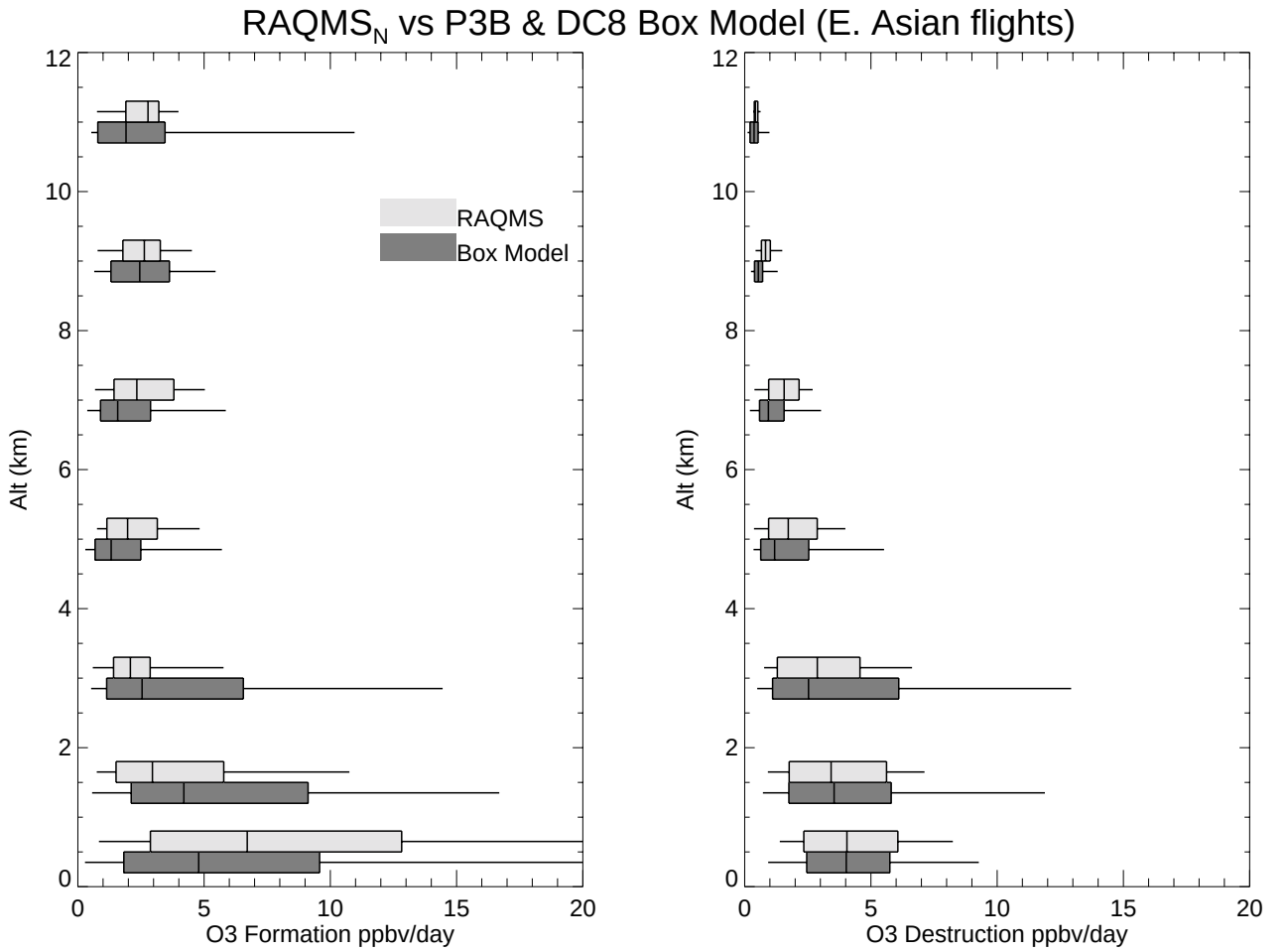
RAQMS$_N$ vs P3B & DC8 Box Model (E. Asian flights)
RAQMS
Box Model
Alt (km)
O3 Formation ppbv/day
O3 Destruction ppbv/day

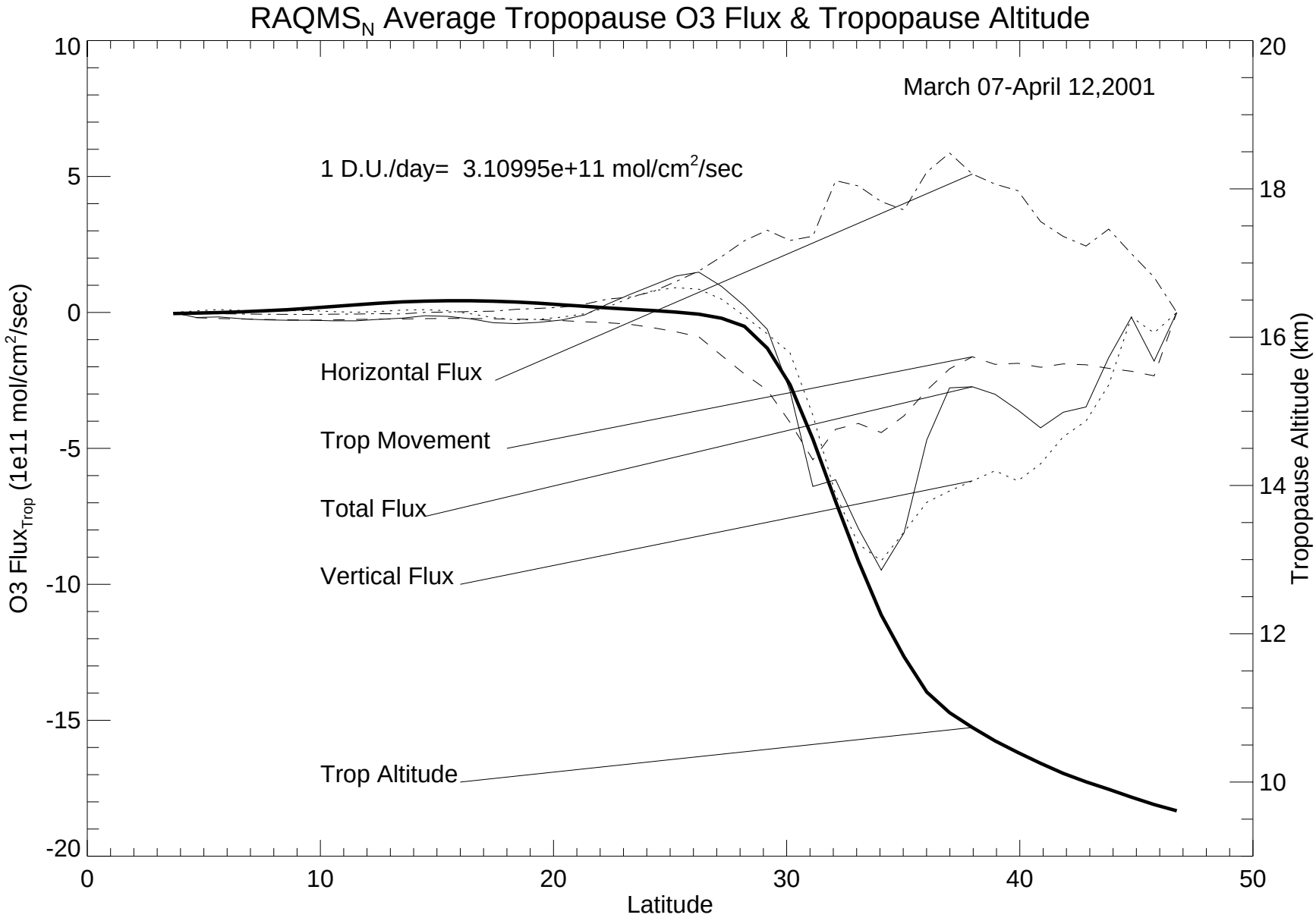
RAQMS$_N$ Average Tropopause O3 Flux & Tropopause Altitude
March 07-April 12,2001
1 D.U./day= 3.10995e+11 mol/cm^2/sec
Horizontal Flux
Trop Movement
Total Flux
Vertical Flux
Trop Altitude
O3 Flux$_{Trop}$ (1e11 mol/cm^2/sec)
Tropopause Altitude (km)
Latitude
10
5
0
-5
-10
-15
-20
20
18
16
14
12
10
0
10
20
30
40
50

Zonal Mean O3 (1e10 mol/cm^3)

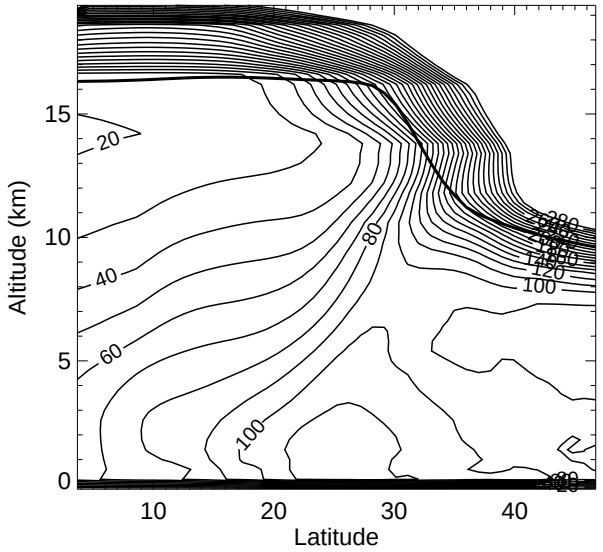

O3 Flux @ West Boundary (1e15 mol/cm^2/s)

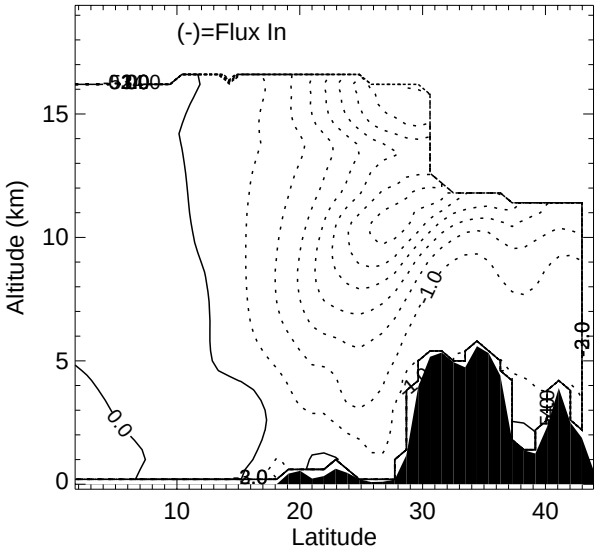

O3 Flux @ East Boundary (1e15 mol/cm^2/s)

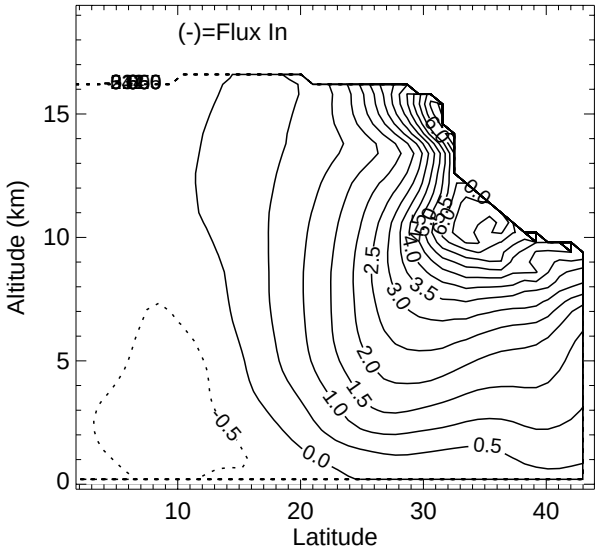

Zonal Mean Net O3 Production (1e5 mol/cm^3/s)

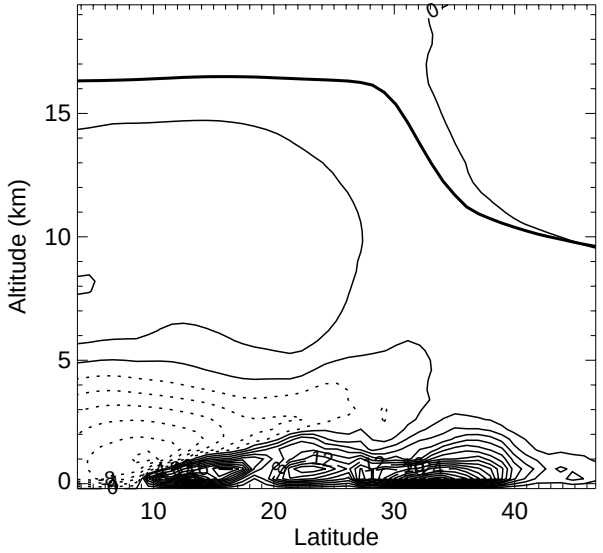

O3 Flux @ South Boundary (1e15 mol/cm^2/s)

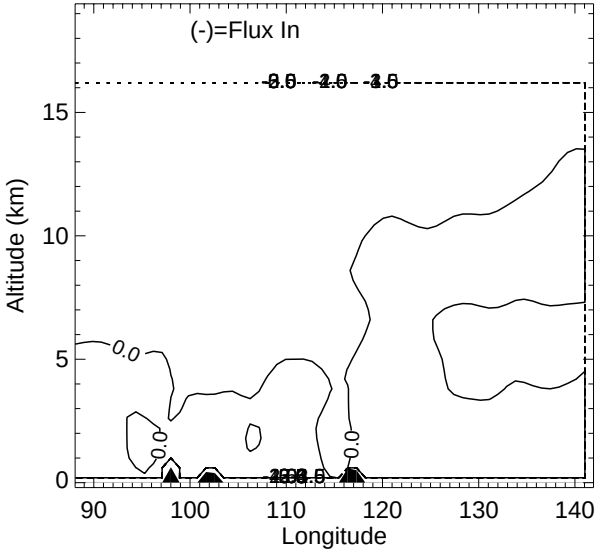

O3 Flux @ North Boundary (1e15 mol/cm^2/s)

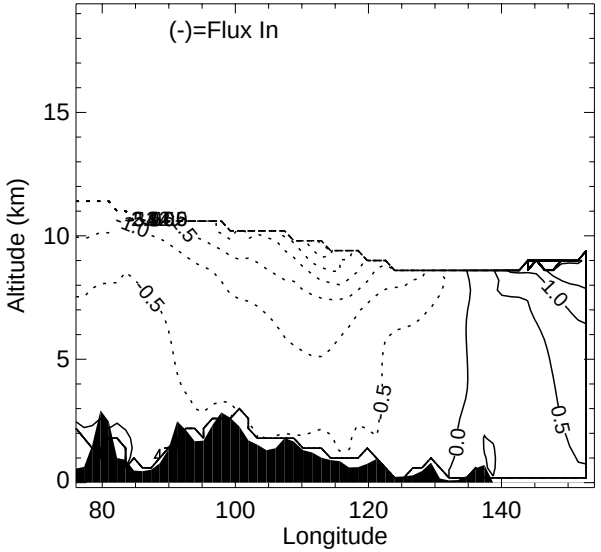

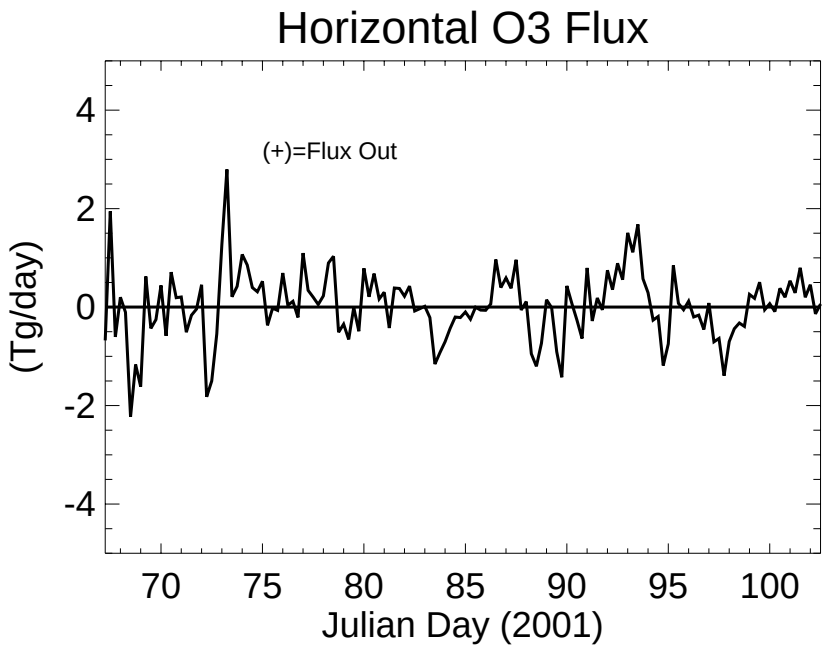
Horizontal O3 Flux
(+)=Flux Out
(Tg/day)
4
2
0
-2
-4
70
75
80
85
90
95
100
Julian Day (2001)

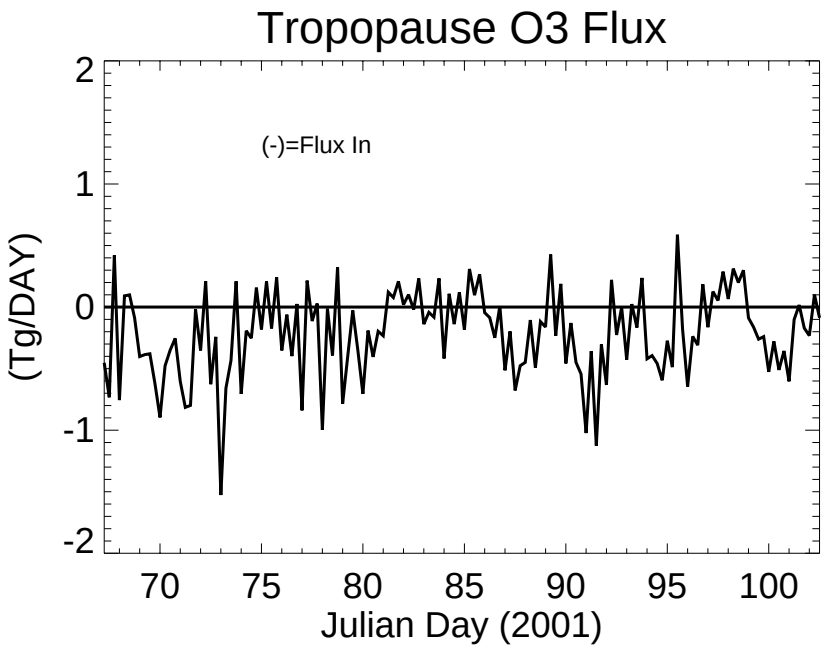
Tropopause O3 Flux
(-)=Flux In
(Tg/DAY)
2
1
0
-1
-2
70
75
80
85
90
95
100
Julian Day (2001)

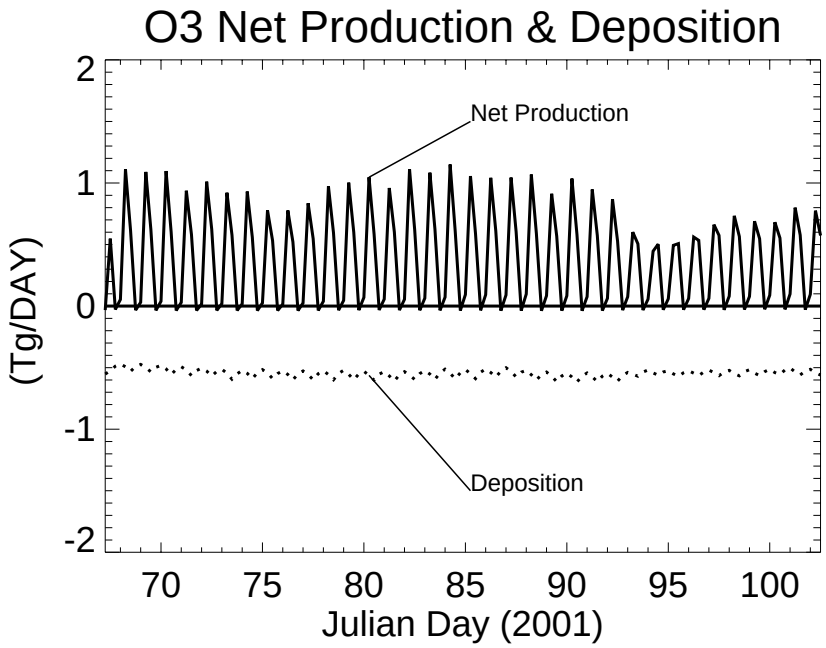
O3 Net Production & Deposition
Net Production
Deposition
(Tg/DAY)
2
1
0
-1
-2
70
75
80
85
90
95
100
Julian Day (2001)

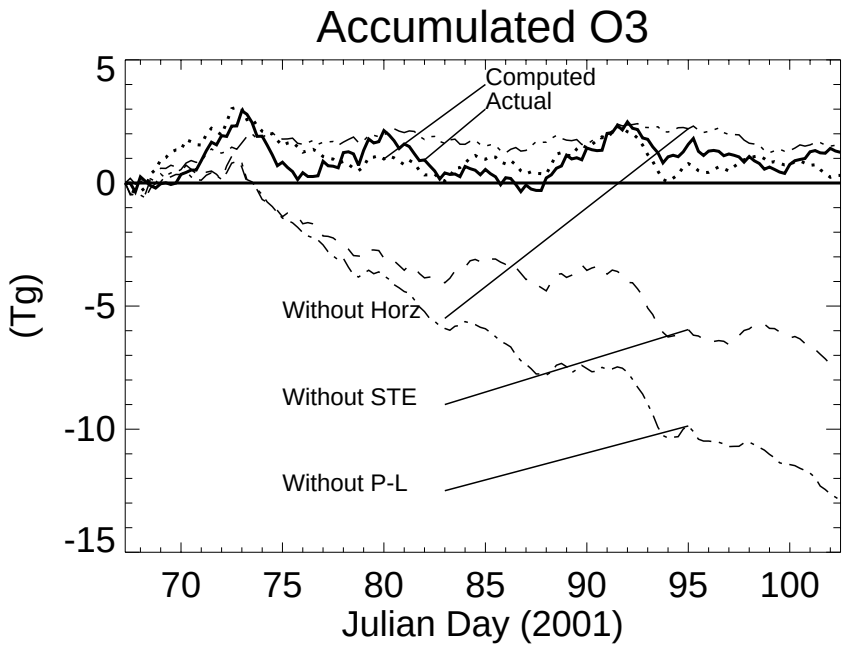
Accumulated O3
Computed
Actual
Without Horz
Without STE
Without P-L
(Tg)
5
0
-5
-10
-15
70
75
80
85
90
95
100
Julian Day (2001)